HYDROGEN TRANSFER DURING COAL LIQUEFACTION DETERMINED BY $^2H/^1H$ MEASUREMENT

Tohru Kamo, James G. Steer, and Karlis Muehlenbachs
Department of Geology
University of Alberta
Edmonton, Alberta, Canada, T6G-2E3

Keywords: liquefaction, hydrogen transfer, isotope

ABSTRACT

Liquefaction of Highvale coal was carried out with tetralin under 6.9 MPa H_2 gas pressure at 400°C and 450°C. The natural ^2H contents of the gas, tetralin, and coal differed substantially and were utilized as tracers of hydrogen transfer. The effect of Fe_2O_3 catalyst, reaction time, and temperature on hydrogen transfer were studied. Products from autoclave tests were separated into light oil, oil, pentane soluble, pentane insoluble - benzene soluble, benzene insoluble - THF soluble, and THF insoluble fractions. At the initial stage of coal liquefaction, hydrogen transfer or exchange between feed gas and coal derived products predominated. But, hydrogen transferred from tetralin was dominant in the more advanced stages of coal liquefaction. Fe_2O_3 catalyst accelerated the interaction between hydrogen gas feed and the coal derived products.

INTRODUCTION

The role of hydrogen is important during coal liquefaction and the control of hydrogen transfer is central to optimizing product distribution. Thus, many attempts have been made to elucidate the mechanisms of hydrogen transfer by deuterium tracer [1] [2], NMR [3] [4] and radioisotope tracer method [5] [6]. Recently, stable isotope methods were used to study coprocessing reactions [7]. In this study, the stable isotope technique was used to identify two separate hydrogen transfer mechanisms during coal liquefaction.

The natural isotopic ratio ($^2H/^1H$) in hydrogen gas, coal and tetralin differ substantially. Products derived from coal have $^2H/^1H$ ratios that may approach either that of tetralin or feed gas identifying the source of the hydrogen. The size of the shifts reflect the relative proportions of hydrogen transfer into coal from gas or tetralin.

EXPERIMENTAL METHODS

Materials. Highvale coal (analysis: C, 71.6; H, 4.4; O, 23.0; N, 0.7; S, 0.3; ash 13.7 wt%, dry basis) was ground to <100 mesh and dried at 110°C for 3 days under vacuum condition. Tetralin, H_2, catalyst (Fe_2O_3) and sulfur were obtained from commercial sources.

Liquefaction procedure. All reactions were done in a 150 ml stirred autoclave. The coal (12g), tetralin (36g), iron oxide (Fe_2O_3, 1.2g), sulfur (0.18g), and H_2 were charged into the autoclave at an initial pressure of 6.9 MPa. The autoclave was heated at 15°C/min and maintained at 400°C and 450°C for 0 min, 60 min and 120 min. For

comparison, tetralin alone, was treated with H_2 and catalyst. After reaction, the autoclave was cooled by blowing air. The volume of gas products was measured and collected in Teflon bags for analysis.

Light oil and oil were obtained by vacuum distillation after filtration of the reaction products. The vacuum residue was extracted to four parts PS (pentane soluble), PI-BS (pentane insoluble - benzene soluble), BI-THFS (benzene insoluble - THFS soluble), and THFI (THF insoluble). A 30 m OV-101 capillary column was used to characterize the liquid products.

Analytical procedure. The feeds and products were analyzed for $^2H/^1H$ by conventional methods of stable isotope geochemistry described previously [7]. The isotopic ratios are determined by isotope ratio mass spectrometry, and the data are reported in the conventional delta notation, relative to the international standard, SMOW.

$$\delta D = ([^2H/^1H] - [^2H/^1H]_{SMOW})/[^2H/^1H]_{SMOW} \times 1000$$

$$[^1H/^2H]_{SMOW} = 1.558 \times 10^{-6}$$

The δD of the coal was -174 ppt, that of tetralin, -105ppt, H_2, -480ppt. The error on replicate analyses was ±3 ppt.

RESULTS AND DISCUSSION

Liquefaction of Highvale coal was carried out in tetralin and H_2. Fig. 1(a) and Fig. 1(b) show the effect of reaction time and the action of Fe_2O_3 catalyst on product distribution at 400°C. THFI decreased with reaction time. Conversion of THFI was a little higher with catalyst than without catalyst. BI-THFS, PI-BS, light oil and gas increased gradually with time. The yield of PS and oil increased slightly with reaction time. These observations indicate that cracking of coal to products lighter than PS was difficult at 400°C. Less light oil and gas were produced when Fe_2O_3 catalyst was added.

The distribution of products from the 450°C runs are shown in Fig. 2(a) and Fig. 2(b). The initial rate of cracking coal was very rapid, nearly 65 % of coal was already converted at 0 min, or when the reactor reached operating temperature. BI-THFS decreased slightly with reaction time without catalyst. With catalyst, BI-THFS gave a low yield already at 0 min. The yield of PI-BS increased at first, but then decreased after 60 min of reaction time. PS, light oil and crack gas increased gradually. The early yield of PI-BS at 450°C was higher than that at 400°C. These trends show that the conversion of coal to PI-BS was rapid and PI-BS was decomposed gradually to PS.

When tetralin was treated without coal but with catalyst at 450°C, naphthalene, 1-methylindan and butylbenzene were produced in small amounts (2.0 wt%, 2.8 wt%, and 1.4 wt%). Therefore, under the experimental conditions, dehydrogenation and decomposition of tetralin was less than 6 wt% in presence of catalyst, and 5 wt% in

absence of catalyst at 450°C. Mainly naphthalene was produced from tetralin during coal liquefaction. 1-Methylindan and butylbenzene were identified in the product. The yield of these compounds in the oil was 1.5 wt% and 4.3 wt% at 400°C and 450°C from the 60 min runs. The δD of tetralin before and after reaction with catalyst at 450°C and 400°C in absence of coal was -105 ppt, -114 ppt and -115 ppt. These small shifts in deuterium content implied no more than 1.5% of hydrogen of the tetralin exchanged with feed gas.

Fig. 3 shows the amount of naphthalene produced in oil at 400°C during coal liquefaction. Naphthalene increased linearly with THFI conversion without catalyst. But, with catalyst, naphthalene increased only gradually. Under this reaction condition, where hydrogenation of naphthalene is very slow [8], the Fe_2O_3 catalyst accelerates hydrogenation of naphthalene back to tetralin. In the tests without catalyst, the amount of naphthalene corresponds to hydrogen transferred from tetralin to coal. Fig. 4 shows hydrogen transfer from tetralin at 450°C. Hydrogen was donated from tetralin to coal when high conversion of coal was achieved.

Fig. 5 shows the δD of the products obtained without catalyst. The δD of products decreased at 400°C with THFI conversion. These products approached the isotopic composition of the feed gas (-480ppt). In contrast, at 450°C, δD of the coal derived products, excluding oil and light oil, increased with THFI conversion. The increase in δD of the higher temperature products reflects hydrogen donation from the tetralin solvent (δD=-105). Fig. 6 shows the isotope ratio of all the product fractions at 0 min of reaction time. The δD of PS, PI-BS, BI-THFS, and THFI were from -190 ppt to -230 ppt. These negative shifts from original δD of Highvale coal (δD =-174 ppt) show that H_2 was more reactive towards coal than was tetralin. More extensive hydrogen exchange was observed in the presence of catalyst.

The δD of products at 60 min are shown in Fig. 7. The δD of fractions from 450°C were higher than that of products at 400 °C. This suggests that at 450°C, hydrogen transfer from tetralin is dominant. The larger shifts of δD with catalyst show that the Fe_2O_3 catalyst accelerated the interaction of H_2 gas and coal. Inspection of the δD values shows that hydrogen from tetralin preferentially reacts with heavier molecular weight fractions THFI and BI-THFS. In contrast, hydrogen in PS and PI-BS reflects more exchange with feed.

These observations show that hydrogen transfer during coal liquefaction proceeds by at least two different pathways. Initially, hydrogen transfer to coal is dominated by absorption of feed hydrogen gas. But, as reactions proceed, hydrogen transfer and exchange between tetralin and coal derived products become increasingly more important. The decrease of δD of the light oils reflect the incorporation of low-^2H feed gas showing

that the light oil was produced by cracking of coal directly followed by hydrogenation with feed gas.

CONCLUSION

1. Two separate mechanism of hydrogen transfer to coal products were identified. Hydrogen transfer from feed gas occurs at the earliest stages of liquefaction whereas hydrogen transfer from tetralin dominates the more extensive, later stages.

2. Fe_2O_3 catalyst accelerated the interaction between hydrogen feed gas and the coal derived products.

3. Hydrogen from tetralin preferentially goes into heavier fraction such as THFI and BI-THFS. Hydrogen in PS and PI-BS is more exchangeable with feed gas.

4. The efficiency of producing products lighter than PS from coal at 400°C was low. When Fe_2O_3 catalyst was added, light oil and gas production was even less. The cracking rate of coal to PI-BS was fast but this fraction gradually decomposed to PS at 450°C.

ACKNOWLEDGEMENTS

We thank Dr. M. R. Gray, Department of Chemical Engineering, University of Alberta, for use of the autoclave and GC and Dr. Y. Sato at National Research Institute Pollution and Resources in Japan for elemental analysis. This work was funded by grants from OCRT of Alberta and the NSERC of Canada.

REFERENCES

1. D. C. Cronauer, R. I. McNei, D. C. Young, and R. G. Ruberto, Fuel, 61, 610 (1982).

2. J. Pajak, Fuel Process. Technol. 23, 39 (1989).

3. M. A. Wilson, P. J. Collin, P. F. Barron, and A. M. Vassallo, Fuel Process. Technol., 5, 281 (1982).

4. R. P. Skowronski, J. J. Ratto, I. B. Goldberg, and L. A. Heredy, Fuel, 63, 440 (1984).

5. T. Kabe, K. Yamamoto, K. Ueda, and T. Horimatsu, Fuel Process. Technol., 25, 45 (1990).

6. T. Kabe, K. Kimura, H. Kameyama, A. Ishihara, and K. Yamamoto, Energy & Fuel, 4, 201 (1990).

7. J. G. Steer, T. Ohuch, K. Muehlenbachs, Fuel Process. Technol.,15, 429 (1987).

8. T. Kabe, O. Nitoh, E. Funastu, K. Yamamoto, Fuel Process. Technil., 14, 91 (1986).

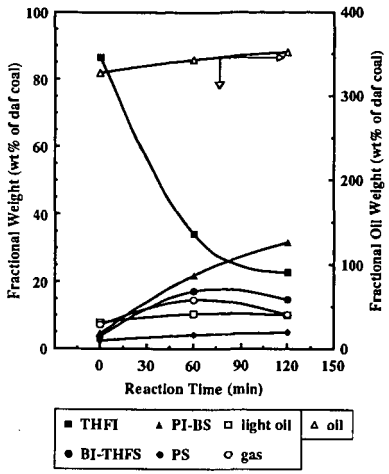

Fig.1(a) Product distribution with catalyst at 400℃.

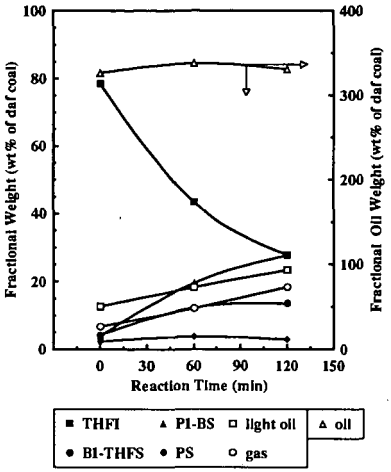

Fig.1(b) Product distribution without catalyst at 400℃.

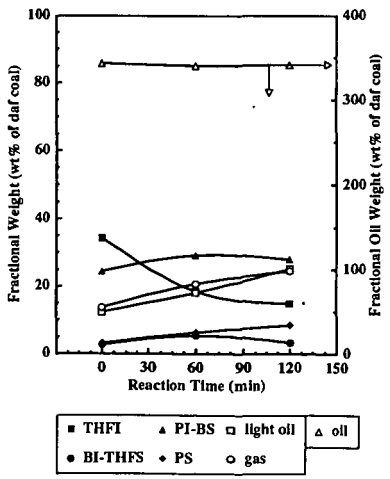

Fig.2(a) Product distribution with catalyst at 450℃.

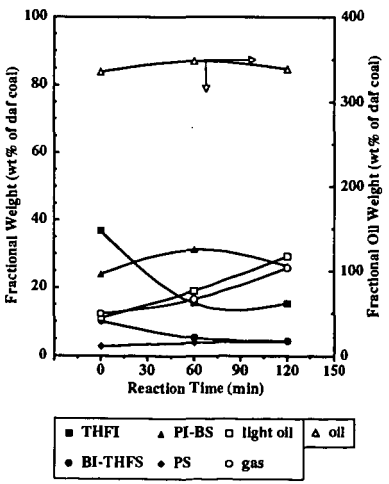

Fig.2(b) Product distribution without catalyst at 450℃.

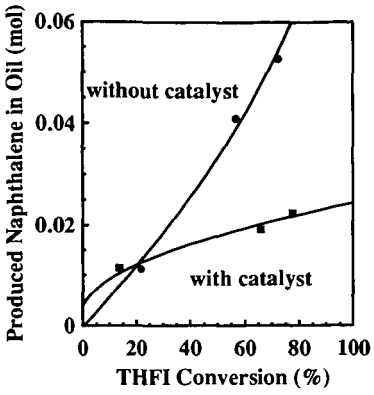

Fig.3 Amount of naphthalene produced in oil at 400°C.

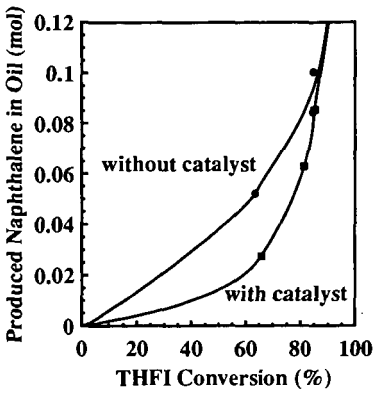

Fig.4 Amount of naphthalene produced in oil at 450°C.

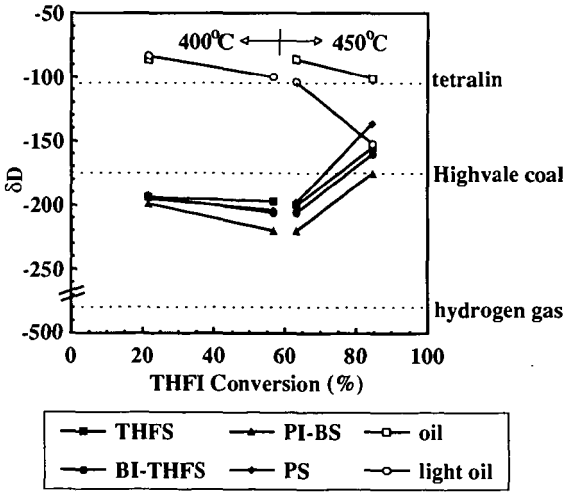

Fig.5 Shifts in $^{2}H/^{1}H$ of products as a function of THFI conversion without catalyst.

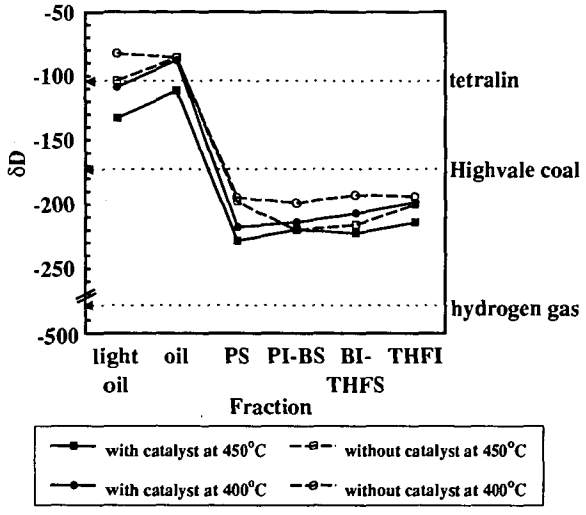

Fig.6 Isotope distribution in products at 0 min

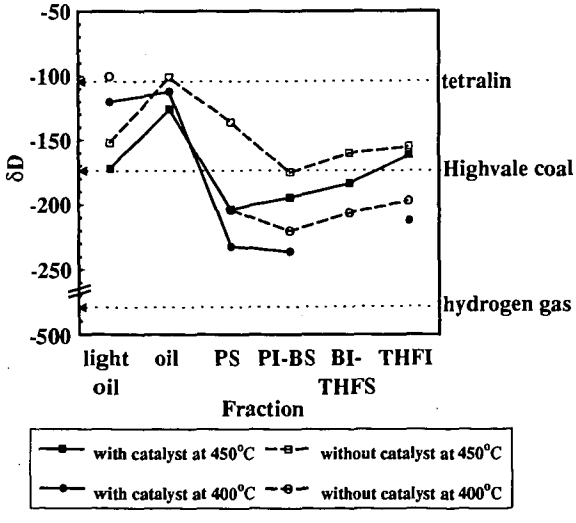

Fig.7 Isotope distribution in products at 60 min

STABLE CARBON ISOTOPE ANALYSIS OF COPROCESSING MATERIALS

Michael S. Lancet, Richard A. Winschel, Francis P. Burke
CONSOLIDATION COAL COMPANY
Research & Development
4000 Brownsville Road
Library, PA 15129

Keywords: Coprocessing, Carbon Isotopes

INTRODUCTION

The purpose of obtaining stable carbon isotope analyses of coprocessing products is to determine the amount of coal (or petroleum) carbon that is present in any reaction product. This *carbon-sourcing* of distillate fractions, soluble resid, and insoluble organic matter, etc. is useful in modeling reactions, and evaluating synergistic effects if they exist. A complete description of the method outlined in this paper, including all experimental details and calculation methods can be found in Reference 1.

Basic Method of Application

In general, the ratio of the two stable isotopes (carbon-12 and carbon-13) differs by small but measurable amounts for different natural hydrocarbons like coal and petroleum. The isotope ratio is reported in units of parts-per-thousand (per mil) difference from a standard. For example, Pittsburgh seam coal has a carbon isotope ratio of about -24 per mil. Cold Lake bitumen has a carbon isotope ratio of about -30 per mil. If we analyze a physical mixture of the two and it has a carbon isotope ratio of, say, -26 per mil, we can use a simple mixing equation to calculate that (-24 - (-26))/(-24 - (-30)) x 100 = 33.3% of the carbon in the mixture is petroleum carbon or, alternatively, that 66.7% is coal carbon. The precision and accuracy of the method are adequate for mixtures of practical interest (2).

Selective Isotopic Fractionation

Actual coprocessing, however, involves considerable bond breaking. Because ^{12}C - ^{12}C bonds are slightly weaker than ^{13}C - ^{12}C bonds, the lighter products, particularly the C_1 x C_4 gases, are slightly enriched in ^{12}C relative to the feed. The heavier products are slightly enriched in ^{13}C. At high conversion conditions (1), this selective isotopic fractionation becomes significant and must be accounted for. The simple physical mixing equation tends to under-account for the isotopically heavier component (usually the coal) in the lighter product fractions, and to over-account for it in the heavier fractions.

PROCEDURES

Sampling and Analysis Procedures

Practical application of stable carbon isotope analysis requires that the coal and petroleum have sufficiently different carbon isotope ratios. In general, a difference of at least 2 per mil is necessary, but a difference of 4 per mil is preferable, particularly if selective isotopic fractionation is expected. With careful attention to sampling and analysis procedures, it is possible to achieve analytical reproducibility (difference between repeat analyses) of about 0.2 per mil routinely. Therefore, the inherent accuracy of the method is about 5% (relative). Without

adequate attention to sampling and analysis procedures it is possible to encounter reproducibility errors of 1 per mil or more, rendering the application essentially useless. The biggest problem appears to be homogeneity for residual samples (i.e., nondistillate oils), although gas samples also are a problem. For viscous liquids and tar samples, the best approach is to homogenize the residual samples by melting, mixing, freezing (in liquid nitrogen), grinding, and remixing, then supplying a small (~1g) aliquot of the sample to the analyst. All isotope analyses were performed at least in duplicate, and an additional replicate analysis was obtained when those results differed by more than 0.2 per mil. Secondary standards similar to the analyzed material should be analyzed routinely to assure accuracy. The standard NBS 22 was analyzed 79 times during this work, giving a standard deviation of 0.04 per mil.

Correcting for Selective Isotopic Fractionation

Selective isotopic fractionation is the most significant problem in applying carbon isotope analysis to carbon-sourcing of coprocessing products. Attempts have been made to account for isotopic fractionation by doing "blank" runs in which the petroleum is processed alone (3). However, it is impossible to do a coal-only run at coprocessing conditions, without the use of a vehicle solvent, and this would require further correction. Ignoring the isotopic fractionation of the coal is convenient; however, we found (1) that higher-rank coals, in particular, undergo significant isotopic fractionation. It is also impractical to do a petroleum-only run and a coal-only run for each coprocessing run. Therefore, we sought a correction method that could be applied for the most common cases in which correction factors from blank runs are unavailable.

The correction method (4,5) is based on the fact that isotopic fractionation will make the hydrocarbon gases isotopically lighter than the respective feed, often by a substantial amount (4-10 per mil relative to the feed). However, because the gas usually represents only a small portion of the carbon (5-10%), the non-gaseous products will differ from the feed by only 0.1 to 1.0 per mil. Therefore, the yield, isotope ratio and carbon content of the gas can be used to calculate the carbon isotope ratios of those portions of the feed coal and feed petroleum that report to the non-gaseous products.

It is not possible to determine from isotope analysis how the coal and petroleum individually fractionate. Overcoming this requires two assumptions. First, we assume that the gaseous carbon is produced from coal and petroleum carbon in equal proportion to their concentrations in the feed. Second, we assume that the degree of fractionation is the same for both feeds. That is, if the isotope balance requires that the gas is 4 per mil lighter than the total feed carbon, we assume that both the coal and petroleum each produce gas that is 4 per mil isotopically lighter than the respective feed carbon. The results of a sensitivity analysis (6) show that, for reasonable relaxations of these assumptions, relative errors are 5-10% if the feedstock pair has a sufficiently large difference in isotope ratio (>4 per mil). A third assumption is that the non-gaseous products from a particular feed all have the same isotope ratio. That is, that the coal-derived carbon in the naphtha has the same isotope ratio as the coal-derived carbon in the resid. In fact, there probably is some heterogeneity in the isotope ratios of the non-gaseous products, with the heavier products being isotopically heavier. This error is minimized by choosing feedstock pairs with large isotopic differences.

It is difficult to obtain valid data on gas samples. However, the carbon content and isotope ratio of the gas can be forced based on the feed analyses and analyses of the non-gas products. If valid gas data are available, they can be used.

EXAMPLE OF APPLICATION TO CONTINUOUS COPROCESSING SAMPLES

This section provides an example of the computations necessary to employ the standard method of correction. The data from five product samples and two feedstock samples from period 11 of Hydrocarbon Research Inc. (HRI) coprocessing Bench Run 238-1, also known as Bench Run No. 2, are used in this example. The feedstocks to this run were Westerholt coal (German bituminous) and Cold Lake vacuum still bottoms (VSB). The large difference, 5.5 per mil, between the isotope ratios of the two feedstocks make the Westerholt coal/Cold Lake VSB pair a good candidate for carbon sourcing via the stable carbon isotope method. The products obtained included initial boiling point (IBP) x 350°F, 350 x 650°F and 650 x 975°F distillates, 975°F$^+$ pressure filter liquid (PFL) and tetrahydorfuran (THF) washed pressure filter cake (PFC). Operating conditions, conversions, and yields (7) from Run 238-1 are given below. A 1:1 MF coal/petroleum ratio was used.

OPERATING CONDITIONS AND PROCESS PERFORMANCE
HRI Coprocessing Bench Run 238-1, Period 11

Conditions	
Feedstock Ratio (dry coal/petroleum):	1
Nominal Pressure, psig:	2500
Temperature, °F (both stages):	810
Relative Space Velocity:	1.0
Process Performance	
Coal Conversion (% MAF):	90
975 °F+ Resid Conversion (% MAF):	82

The input data required for the carbon sourcing calculation are the feed compositions, carbon and carbon isotope analyses of the feed components, and yields, carbon contents, and carbon isotope ratios of the product fractions. These are shown below. As noted above, we found it convenient to calculate the carbon content and isotope ratio of the carbonaceous gas because of problems with sample acquisition and analytical reliability. However, measured values may be used if available. In this example, the gas analyses are calculated by forcing the carbon and isotope analyses. The input data for the example case are given below:

Feed Composition	wt % Feed	wt % Carbon	lb Carbon/ 100 lb feed	$\delta^{13}C$, per mil
Coal (MF)	50.0	77.9	38.9	-24.30
Petroleum	50.0	84.0	42.0	-29.84
Total Feed	100	80.9	80.9	(a)

Feed Composition	wt % Feed	wt % Carbon	lb Carbon/ 100 lb feed	$\delta^{13}C$, per mil
C_1 x C_4, CO_x	12.4	(a)	(a)	(a)
IBP x 350°F	16.1	86.2	13.9	-27.39
350 x 650°F	32.1	87.0	27.9	-27.18
650 x 975°F	19.5	89.2	17.4	-26.12
975°F+ liquid	11.9	91.2	10.9	-25.61
PFC, THF-washed	8.0	66.1	5.3	-23.99
H_2 Consumption	-4.5	-	-	-

(a) Not analyzed.

Based on the feed composition and coal and petroleum analyses, the isotope ratio of the total feed can be calculated as:

$$\delta^{13}C_{feed} = \frac{(-24.30)(38.90) + (-29.84)(42.00)}{80.9} = -27.18 \text{ per mil} \qquad (1)$$

The carbon yield in the product gas is the difference between the feed carbon (80.9 lb) and the sum of the carbon in the other products (13.9+27.9+17.4+10.8+5.3), or 5.6 lb carbon, giving a gas carbon content of 5.6/12.4 x 100 or 45.1%. By forced isotope balance, the isotope ratio of the carbon in the carbonaceous gas is given by:

$$\delta^{13}C_{gas} = \frac{(80.9)(-27.18)-[(13.9)(-27.39)+(27.9)(-27.18)+(17.4)(-26.12)+(10.8)(-25.61)+(5.3)(-23.99)]}{5.6} = -36.0 \text{ per mil} \qquad (2)$$

This illustrates the commonly observed effect of selective isotopic fractionation: the gas (-36.0 per mil) is isotopically lighter (more negative) than either of the feed components.

Based on the calculated carbon isotope ratio of the gas, the isotope ratio of the total non-gaseous product (distillates + resid + PFC) is calculated as:

$$\delta^{13}C_{non\text{-}gas} = \frac{(80.9)(-27.18)-(5.6)(-36.0)}{(13.9 + 27.9 + 17.4 + 10.8 + 5.3)} = -26.52 \text{ per mil} \qquad (3)$$

We assume that the carbon in the product gas is produced from each feedstock in proportion to its carbon in the feed, or 2.7 and 2.9 lb carbon from the coal and petroleum, respectively. We also assume that the difference (X) between the isotope ratio of the coal and petroleum carbon and the gases they produce is the same. X, for each feed, is equal to the difference in the isotope ratio calculated for the product gas and that of the total feed:

$$X = -27.18 - (-36.0) = 8.82 \text{ per mil} \qquad (4)$$

Then the carbon isotope ratios of the non-gas coal and petroleum carbons are calculated as:

$$\delta^{13}C_{coal'} = \frac{(38.9)(-24.3)-(2.7)(-24.30-8.82)}{(38.9 - 2.7)} = -23.64 \text{ per mil} \qquad (5)$$

$$\delta^{13}C_{petr'} = \frac{(42.0)(-29.84)-(2.9)(-29.84-8.82)}{(42.0 - 2.9)} = -29.19 \text{ per mil} \qquad (6)$$

Actually, it was not necessary to calculate the isotope ratio of the gas. The correction to be applied to each of the non-gaseous feedstocks is the difference between the isotope ratio of the total feed (-27.18 from Equation 1) and the total non-gaseous product (-26.52 from Equation 3). These values differ from those of the original feedstocks by 0.66 per mil. Compared to the difference of 5.5 per mil in the coal and petroleum isotope ratios, this represents a relatively small correction. We have documented cases in which isotopic fractionation is more severe, and if feedstock pairs have closer isotope ratios, failure to correct for isotopic fractionation can lead to unacceptably large errors.

To complete the calculation, these corrected values are used in lieu of the original feedstock isotope ratios, to calculate the coal carbon contents of the non-gaseous products. For example, the coal carbon content of the IBP X 350 °F distillate (-27.39 per mil) is given by:

$$\% \text{ Coal Carbon} = \frac{-29.19 - (-27.39)}{-29.19 - (-23.64)} \times 100 = 32.4\% \qquad (7)$$

The remainder of the product compositions are calculated in a similar manner. The results are shown below.

Product Fraction	% Coal Carbon	% Petroleum Carbon
C_1 x C_4, CO_x	48.1	51.9
IBP x 350°F	32.4	67.6
350 x 650°F	36.2	63.8
650 x 975°F	55.4	44.6
975°F+ liquid	64.6	35.4
PFC, THF-washed	93.8	6.2

Conversions

Knowing the relative proportions of coal and petroleum carbon in the product fractions, it is possible to calculate the conversion of either feedstock to that fraction. This could be useful information in reaction modeling, or for investigating the possibility of feedstock synergisms. The conversions from this example are given below:

	Conversion	
Product Fraction	% Coal Carbon	% Petroleum Carbon
C_1 x C_4, CO_x	6.9	6.9
IBP x 350°F	11.6	22.3
350 x 650°F	26.0	42.4
650 x 975°F	24.7	18.5
975°F+ liquid	18.0	9.1
IOM	12.7	0.8
Total	99.9	100.0

Selectivity

The coal-conversion selectivity is simply the ratio of the percent coal carbon in a given product fraction to that in the feed (in this case 48.1%). A value greater than unity indicates that the coal carbon is preferentially converted to (or retained in) that product fraction. Selectivities for this example are given below.

Product Fraction	Coal Carbon Selectivity
IBP x 350°F	0.7
350 x 650°F	0.8
650 x 975°F	1.2
975°F+ liquid	1.3
PFC, THF-washed	2.0

These results indicate that the lower boiling distillates were preferentially produced from the petroleum, while the higher boiling distillates, resid and IOM were preferentially produced from the coal. Note that there is no information on

the gas. We assumed in correcting for selective isotopic fractionation that it was produced with equal selectivity from the coal and petroleum.

SUMMARY

It was demonstrated that, under appropriate circumstances, stable carbon isotope analysis can be an excellent method to determine the contributions of the individual feedstock to coal/petroleum coprocessing products and to follow the reaction pathways of the individual feedstocks. There are two primary considerations in applying this method: 1) the difference in the stable carbon isotopic compositions of the two feedstocks ($\delta^{13}C$), and 2) selective isotopic fractionation errors. An adequate difference in the isotope ratios of the coal and petroleum can be assured by selecting the appropriate coprocessing feedstocks. Selective isotopic fractionation is a consequence of the coprocessing process. It is affected by processing severity, and most coprocessing operations are at high enough severity to induce significant isotopic fractionation. Nevertheless, errors introduced by isotopic fractionation can be corrected, at least in some circumstances.

Even in those cases where the feedstocks are isotopically similar and where isotopic fractionation effects are significant but not corrected (worst case), the method provides data that are useful for discerning trends. However, for use of the method as a quantitative tool, it is important to maximize the difference in the isotope ratios of the coprocessing feedstocks and to follow good, careful sampling and analytical practices. This method allows one to examine the fate of the individual feedstocks through the coprocessing process.

ACKNOWLEDGMENTS

The authors gratefully acknowledge J. E. Duddy and S. V. Panvelker of HRI for supplying the samples and yield data. This work was funded by the U.S. Department of Energy under contract No. DE-AC22-88PC88800.

REFERENCES

1. Winschel, R. A.; Lancet, M. S.; Burke F. P. "Stable Carbon Isotope Analysis of Coprocessing Materials - Final Report" DOE Contract No. DE-AC22-88PC88800, Report No. DOE/PC 88800-43, April 1991.

2. Winschel, R. A.; Lancet, M. S.; Burke F. P. "Stable Carbon Isotope Analysis of Coprocessing Materials - Quarterly Technical Progress Report, July 1 - September 30, 1989". DOE Contract No. DE-AC22-88PC88800, Report No. DOE/PC 88800-26, July 1990.

3. Steer, J. G.; Ohuchi, T.; Muehlenbachs, K.; *Fuel Process. Technol.* 1987, *15*, 429-438.

4. Winschel, R. A.; Burke, F. P.; Lancet, M. S. "Application of Stable Carbon Isotope Analysis to Continuous Coal/Oil Coprocessing", Preprints, Fuel Chemistry Division, American Chemical Society vol. 35, No.4, p 1032, 1990.

5. Burke, F. P.; Winschel, R. A.; Lancet, M. S. "Stable Carbon Isotope Analysis of Coprocessing Materials - Quarterly Technical Progress Report, April 1 - June 30, 1989". DOE Contract DE-AC22-88PC8800, Report No. DOE/PC 88800-25, May 1990.

6. Lancet, M. S.; Winschel, R. A.; Burke, F. P. "Stable Carbon Isotope Analysis of Coprocessing Materials - Quarterly Technical Progress Report, January 1 -

6. Lancet, M. S.; Winschel, R. A.; Burke, F. P. "Stable Carbon Isotope Analysis of Coprocessing Materials - Quarterly Technical Progress Report, January 1 - March 31, 1990". DOE Contract DE-AC22-88PC8800, Report No. DOE/PC 88800-34, December 1990.

7. Duddy, J. E., personal communication to R. A. Winschel, May 9, 1988.

ADVANCED ELECTRON PARAMAGNETIC RESONANCE (EPR) TECHNIQUES FOR THE STUDY OF COAL STRUCTURE

B.G. Silbernagel, M. Bernardo, L.A. Gebhard and H. Thomann
Corporate Research—Exxon Research & Engineering Co
Route 22 East, Annandale, NJ 08801

Keywords: Coal, Electron Paramagnetic Resonance, Double Resonance

INTRODUCTION

Electron Paramagnetic Resonance (EPR) has been extensively applied to the study of coal [1]. In conventional EPR relatively featureless microwave absorptions are observed, from which one extracts the width and position (g–value) of the microwave absorption as well as the density of carbon radicals in the sample. For example, in a conventional EPR study of isolated coal macerals [2], these properties vary with increasing coal rank: g–values fall from values expected for oxidized aromatics to those of aromatic radicals, while radical densities and linewidths generally increase. Microwave saturation techniques (i.e. measuring the intensity of the absorption as a function of applied microwave field) show that high rank coals are much less easily saturated. The relation to the relaxation properties of the carbon radicals is less obvious, since saturation depends on the product of two relaxation parameters of the carbon radicals.

The conventional EPR absorption width results largely from interactions of the unpaired electron spin on the carbon radical with protons in its vicinity, either as a result of direct wave function overlaps (contact interactions) or dipole interactions. Distributions in g–values and dipolar interactions among the carbon radicals themselves will also contribute to the observed width. Identifying and separating these contributions can not be done by conventional EPR alone. The present paper describes two classes of pulsed EPR experiments, analogous to widely–used pulsed NMR techniques: Electron Spin Echo (ESE) determinations of spin–lattice (T_1) and spin–spin (T_2 or T_{m1}) relaxation and double resonance techniques like pulsed ENDOR (Electron Nuclear Double Resonance) [3]. While such techniques can be applied with great effect to relatively homogeneous systems, such as individual compounds or the active sites in enzymes, it is not obvious, *a priori*, that such elaborate schemes will yield useful information in a material as heterogeneous as coal. The present paper will demonstrate the nature of the information that can be obtained and assess its usefulness.

EXPERIMENTAL

The experiments described here have been performed on two series of samples: the isolated coal macerals [2] and a series of "as received" samples of Argonne Premium Coal samples [4]. While there is some concern about the quantitative nature of the data from the "as received" Argonne Premium Coal samples—due to the presence of significant levels of paramagnetic species, the qualitative features are still illustrative. The pulsed EPR experiments were run at microwave frequencies from 9.1–9.4 GHz. The relaxation measurements were performed at room temperature, while the double resonance measurements were done at ~100K. For the double resonance experiments, the rf frequency used to excite the protons was swept from 1–30 MHz.

RELAXATION RESULTS

The relaxation properties of the isolated vitrinite macerals as a function of coal rank probe the interactions of radicals in the coal [5]. Instantaneous diffusion contributes to phase memory loss in higher rank coals and can be separated from the asymptotic phase coherence decay rate, T_{m1}^{-1}, which is the EPR analog of T_2. Values of T_{m1}^{-1} and T_{1e}^{-1} for vitrinites varying in rank from subbituminous C to low volatile bituminous are shown in Fig 1. The T_{1e}^{-1} values are more than an order of magnitude smaller than T_{m1}^{-1} in all cases: spin lattice relaxation is much slower than phase memory loss. The contribution of the dipole coupling to the width of the conventional EPR line can be estimated from the magnitudes of T_{m1}^{-1}, and is much smaller the contributions from hyperfine interactions.

Both T_{1e}^{-1} and T_{m1}^{-1} values are relatively small for low rank coals, with T_{m1}^{-1} beginning to

increase in the vicinity of 78 wt. % carbon, and T_{1e}^{-1} showing a sharp increase near 82 wt. % carbon. The T_{ml}^{-1} values vary nearly linearly with carbon radical density indicating that they result from dipole interactions among the radicals. By contrast, the sharp change in T_{1e}^{-1} does not track radical density and appears related to changes in the local order of the aromatic molecules with increasing coalification.

DOUBLE RESONANCE EXPERIMENTS

Double resonance experiments require that the carbon radicals and the protons be simultaneously excited by microwave and rf pulses. Two of the double resonance schemes, for pulsed ENDOR and EPR detected sublevel coherence, are shown in Fig 2. In each experiment, the electron spin population of the radicals is prepared by the applying microwave pulses and then rf pulses are applied to the protons. At an appropriate time the electron and nuclear spin systems are allowed to mix and the results are detected in the electron spin system. The cavities required to allow simultaneous microwave and rf operations are a challenge to design and construct and remain at the frontiers of the technique development.

Fig 3 shows pulsed ENDOR data on a sample of Pocahontas coal [3]. In one case the ENDOR experiment was performed with the microwave frequency at the absorption center ($g = 2.0026$) and also with the frequency positioned on the low field (i.e. high g–value ≈ 2.0091) portion of the absorption. In each instance, a sharp signal centered at the proton Larmor frequency is seen from "matrix" protons—i.e. those not directly coupled to the radical but interacting with it via dipole interactions. The broader spectrum, which extends at least 15 MHz on either side of the center, comes from "local" protons—i.e. those interacting directly with the moments via some form of wave function overlap. The shape of the local ENDOR signal is nearly identical for all of the high volatile bituminous coal samples observed and has the same shape at 298K and 85K. The ratio of the matrix to local ENDOR signals does vary with rank and temperature, the matrix signals being relatively stronger in the lower rank coals. There is no evidence for major structure in the local ENDOR for any of the samples examined. Fig 3 also shows that the shape of the local ENDOR signal does vary for different positions of the microwave frequency. We suggest that this reflects the different chemical forms of the radical–bearing molecules lying at different places in the resonance line—particularly for the heterocyclic molecules which lie at high g–values.

EPR detected sublevel coherence measures proton dynamics on the carbon radicals, an exciting prospect since magnetic broadening usually renders these protons unobservable by NMR techniques. The protons contributing to the matrix ENDOR have faster T_2 relaxation than those in the local ENDOR component of the signal—presumably a result of field inhomogenieties associated with protons close to the radical.

CONCLUSIONS

Advanced EPR techniques provide new, quantitative information about coal chemistry and its variation with rank. The greater information obtained about interactions on the radical itself should further progress in the understanding of coal microscopics.

REFERENCES

1 Retcofsky, H.L. Coal Science and Technology, Academic, New York, 1982.

2 Silbernagel, B.G., Gebhard, L.A., Dyrkacz, G.R. and Bloomquist, C.A.A. ESR of Isolated Coal Macerals, Fuel, 1986, 65, 558–565.

3 Keijzers, C.P., Reijerse, E.J., and Schmidt J. Pulsed EPR: A New Field of Applications, North Holland, Amsterdam, 1989.

4 Vorres, K.S. The Argonne Premium Coal Sample Program, Energy & Fuels, 1990, 4, 420–426.

5 Thomann, H. Silbernagel, B.G. Jin, H. Gebhard, L.A., Tindall, P. and Dyrkacz,

G.R. Carbon Radical Spin Dynamics in Isolated Vitrinite Radicals, Energy & Fuels, 1988, 2, 333–339.

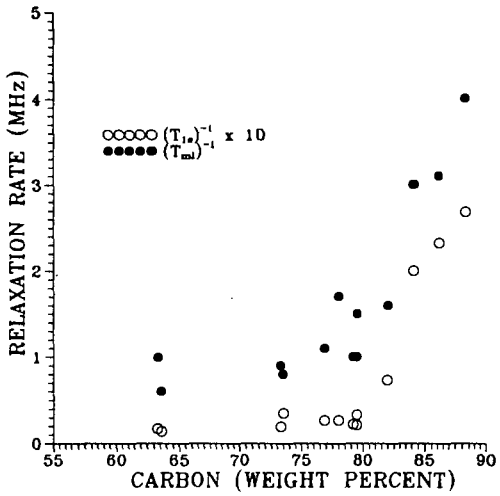

Fig 1 *Relaxation rate measurements on isolated vitrinite macerals [5] show significant increases in both* T_{ml}^{-1} *and* T_{1e}^{-1} *with increasing coal rank.*

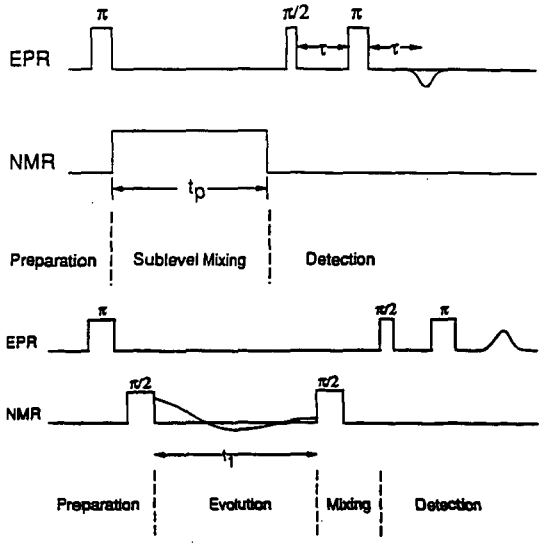

Fig 2 *Double resonance schemes for doing pulsed ENDOR (top) and EPR detected sublevel coherence (bottom) experiments.*

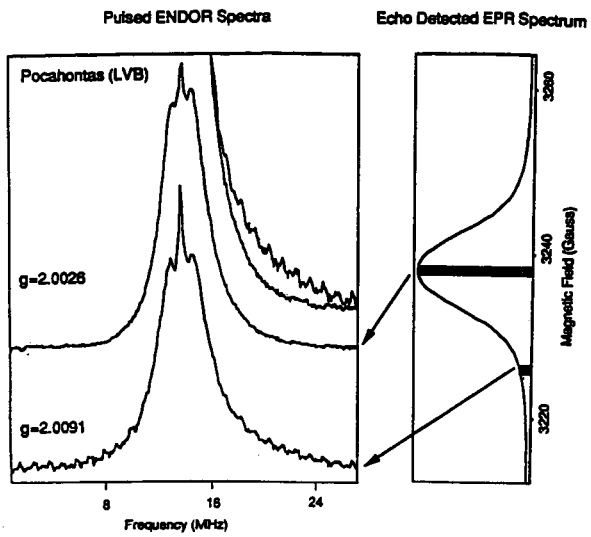

Fig 3 *The ENDOR spectra from the center of the resonance (g = 2.0026) and the low field end (g = 2.0091). Both matrix and local ENDOR signals are observed. The shape of the local ENDOR spectrum is significantly different at high g−value.*

AN INVESTIGATION OF THE CHEMISTRY OF THE PORE STRUCTURE OF COAL IN THE PRESENCE OF A SWELLING SOLVENT USING A NOVEL EPR TECHNIQUE

Dennis R. Spears, Wojciech Sady and Lowell D. Kispert

Box 870336, Chemistry Department
The University of Alabama, Tuscaloosa, AL 35487-0336

KEYWORD: Porosity, coal swelling, EPR, nitroxyl spin probe

ABSTRACT

To study the hydrogen bonding ability of functional groups in pores of Argonne Premium Coal Samples (APCS) exposed during swelling, small nitroxide spin probes with reactive R groups differing in polarity were diffused into APCS coals during swelling and the concentration of the trapped probes measured by an EPR method. As the hydrogen bonding ability of R increases, the degree of probe retention increases; however, probe retention decreases with rank. Polar solvents like pyridine interact specifically with polar functional groups on the micropore wall and prevent binding with polar guest molecules.

INTRODUCTION

The pore structure of coal plays an important role in the behavior of coal during mining, benefaction, and utilization. The pore structure of coal has three components, macropores (>300 Å diameter), mesopores (300 - 12 Å diameter) and micropores (< 12 Å diameter). The micropores make up as much as 88% of the total pore volume of low rank coals and up to 12% of the total pore volume of anthracites (1). Since most of the surface area of coals is located in the micropores (2), rates of reaction are limited by rates of diffusion through the micropore structure.

The micropore structure has been studied by several methods. Helium adsorption is the oldest method(3,4). More recently, small angle x-ray scattering (SAXS) (5,6) and small angle neutron scattering (SANS) (7,8), have been used to examine the micropore structure of coal. The micropore system undergoes changes in the presence of swelling solvents. Gethner showed that weakly swelling solvents such as cyclohexane do not change the micropore structure significantly from the dry state (9). Gethner (8), Winans and Thiyagarajan (7) showed that in the presence of benzene, micropores were spherical in shape. In the presence of pyridine, pores become elongated and cylindrical.

B. G. Silbernagel et. al. (10) first expanded EPR to examine guest molecules incorporated into coal. Silbernagel (10) wanted to study guest molecule inclusion into coals. He used 2,2,6,6-tetramethylpiperidine-1-oxyl, TEMPOL (Figure 1), as a probe. TEMPOL is a stable free radical and gives a highly articulated EPR spectrum. In the presence of coal, the center peak is overlapped by the carbon radical peak. Over several hours, the TEMPOL signal broadens and diminishes. However, the total spin density remains constant during this time, implying that TEMPOL is not being destroyed. The broadening occurs when the rate of motion of TEMPOL molecules drops below the value need for motional narrowing (10^8 sec^{-1}). The restriction of motion implies that, since the TEMPOL is not being destroyed, it must be included in the coal matrix (10).

To study the dynamics of the inclusion process, Silbernagel et al. (10), measured the derivative height of the TEMPOL spectrum as a function of time for Illinois No. 6 hvb coal swelled with benzene. A rapid reduction of the derivative intensity was observed after the first few minutes, indicating that adsorption had taken place. After the first few minutes, the reduction of derivative intensity became slower. A plot of the product of derivative intensity and $t^{1/2}$ versus time indicated that TEMPOL was indeed diffusing into the coal. With these experiments, Silbernagel et al. had developed a unique method for investigating the microporosity of coal (10).

Kispert and coworkers expanded on this technique to study the effect of low temperature swelling on the micropore system of coal. Wu and Kispert (11) showed that a wide variety of spin probes could

be incorporated into coal to study the micropore structure of coal. Cooray (12) studied the mechanism of probe interaction with coal by measuring $2A_{zz}$ as a function of temperature. Cooray concluded that at temperature above 220 K the spin probes exhibited no significant interaction with coal (12). Goslar and Kispert (13) conducted electron double resonance spectroscopy (ENDOR) on coals doped with nitroxyls and confirmed the absence of significant coal-spin probe interaction, at least through the N-O bond.

The effect of low temperature swelling conditions on pore size and shape has been extensively studied by Spears et al. (14,15). Coals contain spherical pores when swelled at low temperature and with a mild swelling solvent. Upon swelling with hydrogen bonding solvents such as nitrobenzene or pyridine, pores become elongated and cylindrical. The degree of elongation is dependent on both the polarity of the swelling solvent and the swelling temperature. To determine the number of spherical probes present TEMPOL was used as a spin probe. TEMPOL, although spherically shaped, has an -OH group which could potentially interact with the coal. Gethner has recently shown that pore walls in coal are covered with oxygen functionalities. (16) Although it was known that nitroxyls did not interact significantly at 300 K with coal through the N-O bond, it was thought that the polar R group of TEMPOL might.

To understand the chemistry of the micropore walls, a series of similarly sized nitroxyls were incorporated into the micropore structure of Argonne Premium Coal Sample (APCS) coals. The effects of rank, swelling solvent polarity, swelling temperature, and drying of the coal were investigated.

EXPERIMENTAL

The experimental procedure has been described elsewhere in detail (11-15). Spin probes were imbibed into the pore structure of coal in the presence of a swelling solvent. The solvent was removed, causing the pore structure to collapse about the incorporated nitroxyls. The coal was then washed with cyclohexane. If the spin probe was unable to penetrate a pore because it had not swelled open sufficiently, it was removed in the cyclohexane wash. If the probe molecule was trapped in a pore much larger in size, it was also removed in the cyclohexane wash. Thus, after the cyclohexane wash, all probes retained were trapped in pores similar in size and shape to the nitroxyl molecule.

The general structural shape of the spin probes used in this study are shown in Figure 1 where R represents the substitutent for each spin probe. The specific spin probes are numbered in the same manner as defined previously (12). Spin probe VIII, 2,2,6,6-tetramethylpiperidine-1-oxyl, is the basic structural unit for all nitroxyl spin probes studied. Spin probes VIII, I, VI, and VII are similar in size (molecular volume approximately 140 $Å^3$) and are spherically shaped. Spin probe X is larger (molecular volume 310 $Å^3$) and cylindrically shaped. All eight APCS coals were studied (Table 1). Coals were swelled in either toluene or pyridine at 333 K for 18 hours. Spin probe concentration was determined by EPR and normalized to 1 g of coal.

DISCUSSION

The number of spherically shaped micropores was determined by imbibing spin probe VIII into coal. Spin probe VIII should exhibit no significant interaction with coal. The results of swelling coal at 333 K with solutions of spin probe VIII are shown in Figure 2 as a function of rank and swelling solvent. Carbon content was used as convenient rank indicator throughout this study. For coals swelled in toluene, the number of small, spherically shaped pores is small such as for Beulah-Zap lignite and Wyodak subbituminous coals (74 and 76% carbon, dmmf, respectively), and quickly fall to zero as rank increases. In pyridine at 333 K, none of the APCS coals retained spin probe VIII. This indicated that all of the small, spherically shaped micropores had vanished.

Comparing the results with spin probe X, a spin probe larger than spin probe VIII and cylindrical in shape, shows that the micropores are enlarged and elongated. Figure 3 shows the change in spin probe X and VIII concentration with carbon content for coals swelled in either toluene at 333 K. The coals retained larger concentrations of spin probe X than spin probe VIII. This showed that the micropores were indeed becoming elongated.

Pore elongation in swelled coals meant that coals should not retain significant amounts of small, spherically shaped pores. However, previous data showed that coals swelled in toluene retained significant amounts of spin probe I and 333 K, especially compared to spin probe VIII. The main

difference between spin probe VIII and spin probe I was the polar R group. Thus the retention in coal was due to association of the -OH group with the pore walls.

Micropore walls, especially in swollen coals, are covered with polar functionalities. Gethner showed that micropore walls in low rank coals were linked with carboxylic acid groups (16). Coals contain significant amounts of hydrogen bonding. Hydrogen bonding in coal has been attributed to oxygen-containing functional groups. The swelling of coal in polar solvents has been ascribed to the disruption of these bonds by solvent molecule interaction. As polar functionalities are exposed by the swelling solvent, spin probes with polar R groups should be retained. The degree of retention should be directly related to the hydrogen-bonding ability of the R group. As the hydrogen-bonding ability of the R group increased, the strength of the spin probe-coal interaction should increase.

To test this hypothesis, APCS coals were imbibed with 4 spin probes differing in the polarity of the R group in toluene at 333 K. The R groups were -H, -OH, $-CO_2H$, and $-NH_4$ (spin probes VIII, I, VI, and VII respectively). The results are shown in Figure 4. As the relative R group polarity increased, the degree of retention increased, especially for low rank coals. Although the micropore system was enlarged by toluene swelling at 333 K, polar spin probes were still retained. This indicated that spin probes with polar R groups were retained in macropores larger than the size of probe molecule itself. Retention was apparently due to interaction of the polar R group with the coal surface. This mechanism of retention was considerably different from the simple physical entrapment for other spin probes studied (11-15).

The polarity of the functional groups in the micropore walls is apparently low. Highly polar functionalities should show little specificity of retention between the spin probes studied. A knowledge of the dissociation constants or the electron donor numbers of the spin probes should give more specific details as to the polarity of coal function groups.

Low rank coals contain larger quantities of oxygen functionalities and so should retain more of polar spin probes. The degree of retention decreased with rank, and the influence of R group polarity decreased with rank, but even at the highest ranked APCS coals, the effect of R group polarity was still significant. These results showed that polar functionalities were still present even at high rank coals. These functionalities are likely responsible for the hydrogen bonding which earlier spin probe studies had indicated that existed in coal of all ranks (15).

If hydrogen bonding was indeed a factor in the coal tertiary structure, then swelling coal in pyridine at 333 K would disrupt the hydrogen bonding network considerably. Previously results showed that swelling coal in pyridine at 333 K caused considerable opening of the micropore structure (15). This could only be the result of disruption of the hydrogen bonding network. Such disruption, followed by solvent removal, could lead to the exposure of polar functionalities within the coal, and result in greater retention of polar spin probes.

To test this hypothesis, APCS coals were imbibed with 4 spin probes differing in the polarity of the R group in pyridine . The R groups were -H, -OH, $-CO_2H$, and $-NH_2$ (spin probes VIII, I, VI, and VII respectively). The results are shown in Figure 5. As for coals swelled in toluene, an increase in the relative R group polarity resulted in increased retention although the difference between spin probe VI and spin probe VII is negligible. However, a comparison of Figure 4 with Figure 5 shows that, for a given spin probe, coals swelled in pyridine retained fewer spin probes than coals swelled in toluene, contrary to expectations.

Green showed that molecules capable of hydrogen bonding interact with specific sites in coal. (17) Pyridine interacts strongly with coal, and is not entirely removed even under the most severe vacuum drying. It is possible that unremoved solvent molecules tied up existing hydrogen bonding sites, reducing the number of sites available for spin probe-coal interactions. If many of the reactive sites in coal are tied up, then the polar spin probes would be trapped in enlarged micropores with fewer sites available for specific interaction. This would result in removal during the cyclohexane wash. To examine the swelling characteristics of the APCS coals after drying, APCS coals are now being subjected to vacuum drying at either room temperature or at 100°C. Results of these studies will be presented.

CONCLUSION

In conclusion, micropore enlargement occurs as the degree of swelling increases. The micropore structure is held together by hydrogen bonding, which can be disrupted by swelling with polar solvents. The micropore walls contain polar functional groups. The number of these functional groups decreases with rank. Polar solvents like pyridine interact specifically with these sites and prevent them from bonding with polar guest molecules. Thus, using a strongly polar solvent to swell coal in conversion processes might actually defeat the purpose by tying up reactive sites.

REFERENCES

1. Gan, H.; Nandi, S. P.; Walker, P. L., Jr. *Fuel* **1972**, *51*, 272.
2. Mahajan, O. P.; Walker, P. L., Jr.; in *Analytical Methods for Coal and Coal Products*, C. Karr, ed., Academic, New York, **1978**, 162.
3. Nelson, J. R., Ph. D. Dissertation, Pennsylvania State University, State College, **1979**.
4. Fuji, S.; Tsuboi, H. *Fuel* **1967**, *46*, 361.
5. Spitzer, Z.; Ulicky, L. *Fuel* **1976**, *50*, 21.
6. Lin, J. S.; Hendricks, R. W.; Harris, L. A.; Yust, C. S. *J. Appl. Crystallogr.*, **1978**, *11*, 621.
7. Winans, R. E.; Thiyagarajan, P. *Am. Chem. Soc. Div. Fuel Chem. Prepr.* **1987**, *32*, 227.
8. Gethner, J. S. *J. Appl. Phys.* **1986**, *59*, 1068.
9. Gethner, J. S. *Am. Chem. Soc. Div. Fuel Chem. Prepr.* **1987**, *32*, 239.
10. Silbernagel, B. G.; Ebert, L. B.; Schlosberg, R. H.; Long, R. B. *Adv. Chem. Ser.* **1979**, *192*, 23.
11. Wuu, S. K.; Kispert, L. D. *Fuel* **1985**, *64*, 1681.
12. Cooray, L. S.; Kispert, L. D.; Wuu, S. K. *Am. Chem. Soc., Div. Fuel Chem. Prepr.*, **1988**, *33*, 32; Cooray, M. L. S., M.Sc. Thesis, University of Alabama, Tuscaloosa, 1988.
13. Goslar, J.; Kispert, L. D. *Fuel*, **1990**, *69*, 564.
14. Spears, R.; Goslar, J.; Kispert, L. D. in *Techniques in Magnetic Resonance for Carbonaceous Solids*, Botto, R., and Sanada, Y., eds., ACS Symposium Series No. 229, In Press.
15. Spears, R.; Kispert, L. D.; Piekara-Sady, L. *ACS Div. Fuel Chem. Prepr.* **1991**, *36*, 29.
16. Gethner, J. S. *Am. Chem. Soc. Div. Fuel Chem. Prepr.* **1987**, *32*, 239.
17. Green, T. K.; West, T. A. *Fuel* **1986**, *65*, 298.

Table 1. Major element composition of Argonne Premium Coal Samples, dmmf basis.

Coal	% C	% H	% N	% S	% O
Upper Freeport	88.08	4.84	1.60	0.76	4.72
Wyodak-Anderson	76.04	5.42	1.13	0.48	16.90
Illinois No. 6	80.73	5.20	1.43	2.47	10.11
Pittsburgh No. 8	84.95	5.43	1.68	0.91	6.90
Pocahontas	91.81	4.48	1.34	0.51	1.66
Blind Canyon	81.32	6.81	1.59	0.37	10.88
Lewis-Stockton	85.47	5.44	1.61	0.67	6.68
Beulah-Zap	74.05	4.90	1.17	0.71	19.13

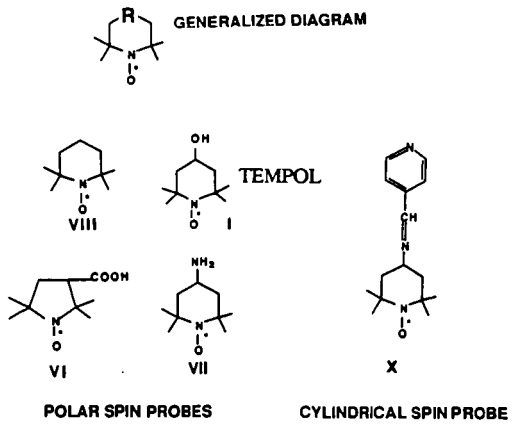

Figure 1. Nitroxyls used as spin probes in this study: A generalized diagram of a nitroxyl molecule is listed as well as; VIII, 2,2,6,6-tetramethylpiperidine-1-oxyl, R = -H; I, 4-hydroxy-2,2,6,6-tetramethylpiperidine-1-oxyl, R = -OH; VI, 3-carboxy-2,2,5,5-tetramethyl- pyrrolidine-1-oxyl, R = $-CO_2H$; and VII, 4-amino-2,2,6,6-tetramethylpiperidine-1-oxyl, R = $-NH_2$; X, Cylindrical nonpolar spin probe, amino-2,2,6,6-tetramethylpiperidine-1-oxyl 4-pyridine carboxaldimine.

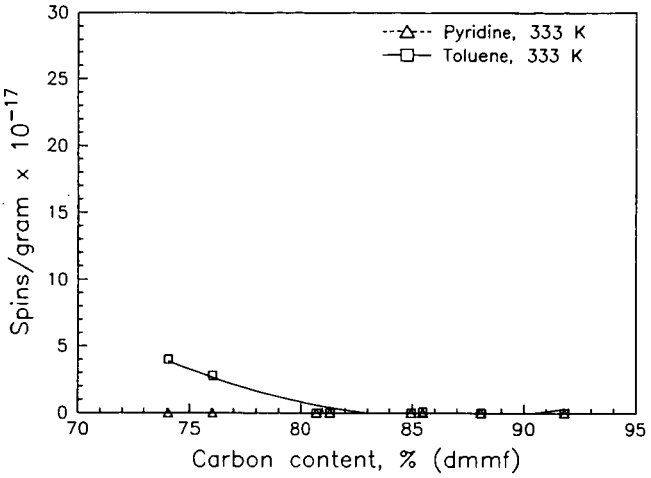

Figure 2. Effect of solvent on the quantity of spherically shaped micropores in coal. Spin probe VIII concentration (spins/g x 10^{17} in coals swelled at 333 K in either toluene (□) or pyridine (Δ) versus rank as % carbon on a dry, mineral matter-free (dmmf) basis.

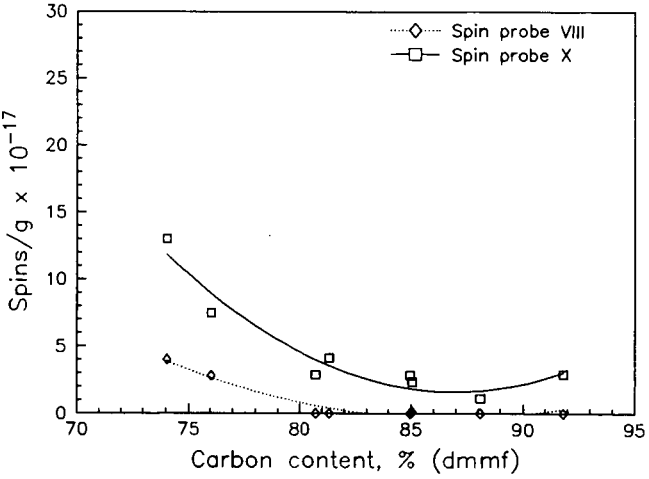

Figure 3. Effect of solvent swelling on micropore shape/size. Spin probe X (□) and spin probe VIII (◊) concentration (spins/g x 10^{17}) in coals swelled in toluene at 333 K, vs. carbon content (%, dmmf).

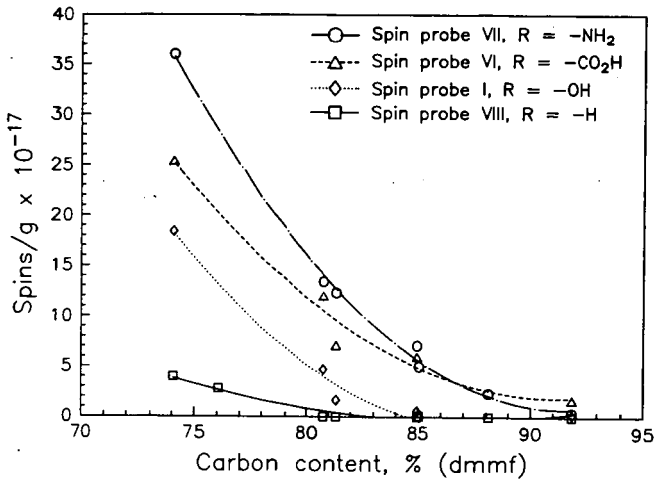

Figure 4. Effect of spin probe R group on spin probe retention in coal for coals swelled in toluene at 333 K. Spin probe VIII, R = -H, (□); spin probe I, R = -OH, (∧); spin probe VI, R = $-CO_2H$, (Δ); and spin probe VII (O)R = $-NH_2$; concentration (spins/g x 10^{-17}) vs. carbon content (%, dmmf).

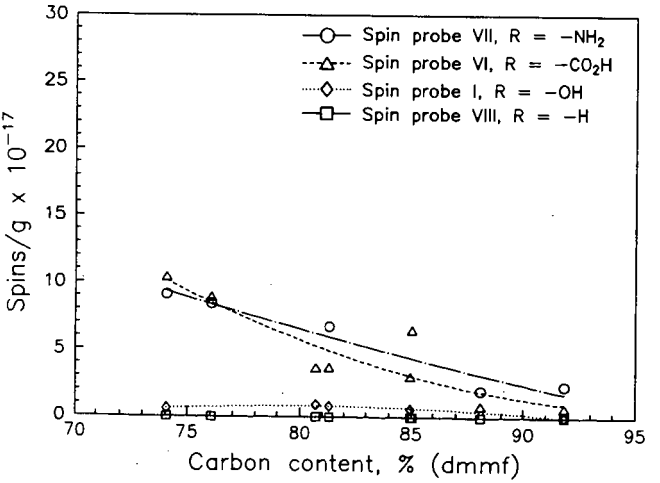

Figure 5. Effect of spin probe R group on spin probe retention in coal for coals swelled in pyridine at 333 K. Spin probe VIII, R = -H, □; spin probe I, R = -OH, (◊); spin probe VI, R = $-CO_2H$, (Δ); and spin probe VII(O)R = $-NH_2$; concentration (spins/g x 10^{-17}) vs. carbon content (%, dmmf).

VERY HIGH FREQUENCY EPR SPECTROSCOPY AND NMR IMAGING OF COAL

R. B. Clarkson, K. Motsegood, W. Wang, A. G. Webb, and R. L. Belford
Illinois EPR Research Center, University of Illinois, Urbana, IL 61801

Keywords: EPR, MRI, organic sulfur, solvent swelling

INTRODUCTION

Last year we began a program to develop and apply Very High Frequency Electron Paramagnetic Resonance (VHF EPR) to non-destructively analyze for organic sulfur molecular forms in coal and separated macerals. The starting point of our work was a preliminary observation that when EPR spectra of coal were taken on our newly constructed VHF spectrometer [1], signals related to organic sulfur were observable. These spectral features could only be resolved at high magnetic fields, and hence had gone undetected in all previous EPR studies of coal, although their presence had been inferred from indirect evidence [2]. Figure 1 clearly shows the resolution of sulfur-related features in an Illinois #6 whole coal at 96 GHz. We also began to develop magnetic resonance imaging techniques to non-destructively assess the effects of various solvents on coal, including the measurement of solvent swelling and solvent penetration. In this report we will discuss recent progress made in both of these areas.

VHF EPR ANALYSIS

What makes the discovery of sulfur-related peaks in the VHF EPR spectra of coal useful as well as interesting is the fact that spectra like that shown in Fig. 1 have the potential to be understood theoretically, thus allowing for the development of a technique which can be analytical for organic sulfur in coal. Furthermore, information from organic sulfur model compounds like dibenzothiophene and benzonaphthothiophene, shown in Figure 2, allow theory to be tested on ideal molecular systems with properties thought to be very similar to those of whole coal. We have developed chemical techniques to synthesize stable cation radical forms of such coal model sulfur compounds, utilizing either (i) boric acid glass matrix isolation followed by UV irradiation, or (ii) formation by electron transfer on catalytically active silica-alumina surfaces [3]. Spectra from compounds such as these form the basis of our interpretation of the more complex spectra obtained from coal.

Three examples will be given to illustrate some of the potential in the VHF EPR method, and the rationale of our approach. The first, shown in Figure 3, compares the VHF EPR spectra of vitrinite and sporinite macerals separated from an Illinois #6. Careful destructive chemical analysis suggests that the vitrinite contains 2.9% organic sulfur, while the sporinite contains 4.3%. Analysis of the VHF EPR spectra of these two samples on the basis of a two-species model, involving the summation of spectra from sulfur and non-sulfur containing species indicates almost identical sulfur levels as obtained by chemical analysis [4]. While the two-species model seems crude, it has proven to be quite useful in analyzing VHF EPR coal spectra, and may represent a reasonable generalization regarding the classes of organic molecular forms contributing to the spectral lineshape. We suggest that at 96 GHz, spin-orbit coupling between unpaired electrons and aromatic sulfur produces the downfield shifts which we resolve in spectra from high-sulfur coal; similar SO coupling effects from oxygen species produce shifts too small to be resolved at this frequency. In collaboration with Prof. Jack Freed (Cornell University), we have examined samples at 250 GHz, and there see lineshapes which may allow a more detailed analysis of

heteratom (S,O) effects.

Figure 4 compares two "before and after" samples in order to study the effects of two desulfurization methods on an Illinois #6. In Figure 4(a), the coal was subjected to extraction with perchloroethylene (PCE) at 120°C for 3.5 hours. As can be seen by inspection, very little changed in the VHF EPR spectra as a result of this treatment, suggesting that little organic sulfur (of the aromatic variety to which our method is believed to be sensitive) was removed, in agreement with D. H. Buchanan and co-workers, from whom the samples were obtained [5]. Figure 4(b) shows spectra of the Illinois #6 before and after low temperature (285°C) pyrolysis for two hours under vacuum conditions ($P < 10^{-5}$ Torr). The greatly reduced low-field peak ($g = 2.00434$) in the pyrolyzed coal suggests that this treatment significantly altered and removed aromatic organic sulfur, as has been reported by Kruse and Shimp [6]. We currently are employing VHF EPR to study the effects of low-temperature pyrolysis on coal structure, and have observed complex spectral changes which need to be understood before a complete interpretation of these effects can be made.

Figure 5. shows VHF EPR spectra of the two model compounds in Figure 2. One primary difference between DBT and BNT is that DBT contains 12 aromatic carbons, while BNT contains 16. As the figure illustrates, this difference of four atoms has a large effect on the spectral lineshape. One component of this sensitivity of lineshape to aromatic ring size is that the g-anisotropy brought about by spin-orbit interactions ($\lambda\ \mathbf{L} \cdot \mathbf{S}$) depends strongly on the unpaired electron spin density on sulfur. As aromatic ring size increases and the unpaired electron delocalizes over a larger carbon skeleton, density on sulfur decreases, resulting in diminished anisotropy, which agrees with the changes seen in the spectra of Fig. 5. We currently are studying a series of thiophenic compounds with varying aromatic ring sizes, in order to develop this theory further.

NMR IMAGING OF SOLVENTS IN COAL

Nuclear magnetic resonance imaging (MRI) can be used in a completely non-invasive way to visualize and measure the changes in pore size as coal is swollen with organic solvents. Preliminary experiments have been carried out using two separate radiofrequency and gradient coil configurations in order to determine the feasibility of studying solvent diffusion into coal samples. The imaging system used is the SISCO 200/330 imaging spectrometer system, located in the Biomedical Magnetic Resonance Laboratory at the University of Illinois/Urbana. This instrument operates at a field strength of 4.7T (ν(proton) = 200 MHz). The first approach used the system's 8 cm. inner diameter double saddle radiofrequency probe as the transmit and receive coil, with the system's magnetic field gradients being driven by Oxford gradient amplifiers to give a maximum gradient strength of 2 G/cm. Additional work now is being carried out using an imaging probe from Doty Scientific, consisting of a solenoidal radiofrequency probe of inner diameter 1.5 cm., and maximum gradient strength of 15 G/cm., when driven by three Techron power supplies.

Samples were obtained from the Illinois State Geological Survey. First, the coal sample was immersed in water, doped with manganese chloride, in order to reduce solvent proton T_1 to 400 msec, and allowed to soak for a week. MRI images then were taken. The water then was removed, and the sample was placed in acetone, doped with 10 mM chromium acetoacetonate (AcAc) in order to reduce solvent proton T_1 to 400 msec. After 48 hours of immersion, the sample was again imaged. Lastly, the acetone was removed, and the sample was immersed in DMSO, again doped with chromium AcAc. After another 48 hours of soaking, a third set of images were obtained.

Figure 6. shows a series of five images from a multislice data set obtained on a sample of Illinois #5 coal (Galatin County, IL), with dimensions of 19 x 19 x 38 mm. Since coal is not swollen by the water, these images define the outer surface of the pre-swollen coal, providing a

reference for subsequent swelling experiments. Each image represents a slice through the coal sample with an in-plane thickness of 1 mm. In plane spatial resolution is 500 microns.

Figure 7. shows the same coal sample after immersion in doped acetone. Some swelling and permeation of the solvent into the coal sample is clearly seen, although the covalent cross-linking in the coal is not yet being substantially broken. Figure 8. follows the same sample after 48 hours of immersion in doped DMSO. The images clearly show significant pore enlargement and swelling of the coal. It should be remembered that these images are internal views of the solid sample, permitting non-destructive analysis, and hence sequential solvent studies on the same piece of coal.

MRI results agree qualitatively with those obtained using methods where no spatial localization or visualization was possible. Estimates of the swelling ratio, Q, for our coal sample in DMSO and acetone, made from the images in Figs. 7 and 8, yield a value of 1.9. Szeliga and Marzec obtained a value of Q = 1.6 for these solvents in a similar coal [7]. These authors have shown that swelling and solvent electron-donor number (defined as the negative of the enthalpy change for the interaction of the solvent with $SbCl_5$ in a dilute solution of dichloroethane) show a reasonably strong correlation, and they discuss the solvents used in our MRI work. Brenner has shown that initial swelling is rapid, although weeks or even months may be necessary to reach equilibrium swelling [8]. He concluded that access of solvent to the sites where swelling is induced is highly variable: some pathways are accessible to the solvent molecules in seconds, others may take days. In the future, we hope to further develop MRI methods to follow these processes in greater detail.

ACKNOWLEDGEMENTS

Partial support for this work was provided by the U.S. Department of Energy (University Coal Research Program, DE-FG22-88PC88921), the Illinois Department of Energy and Natural Resources (Center for Research on Sulfur in Coal, SENR CRG91 CLARKSON), and the National Institutes of Health (RR 01811).

REFERENCES

1. R. B. Clarkson, W. Wang, M. J. Nilges, and R. L. Belford, in *Processing and Utilization of High-Sulfur Coals III*, R. Markuszewski and T. D. Wheelock, eds, Elsevier, Amsterdam, 1990, pp. 67 - 78.

2. H. L. Retcofsky, M. R. Hough, M. M. Maguire, and R. B. Clarkson, in *Coal Structure*, M. L. Gorbaty and K. Ouchi, eds., ACS Advances in Chemistry No. 192, 1981, 37 - 58.

3. R. B. Clarkson, R. L. Belford, K. S. Rothenberger, and H. C. Crookham, *J. Catalysis*, 1987, ***106***, 500.

4. R. B. Clarkson, W. Wang, D. R. Brown, H. C. Crookham, and R. L. Belford, *FUEL*, 1990, ***69***, 1405.

5. D. H. Buchanan, K. J. Coombs, C. Chaven, C. W. Kruse, and K. C. Hackley, in *Processing and Utilization of High-Sulfur Coals III*, R. Markuszewski and T. D. Wheelock, eds., Elsevier, Amsterdam, 1990, pp. 79 - 87.

6. C. W. Kruse and N. E. Shimp, in *Coal Processing Technology, v. VII*, AIChE., 1981, 124.

7. J. Szeliga and A. Marzec, *FUEL*, 1983, ***62***, 1229.

8. D. Brenner, Am. Chem. Soc. Div. Fuel Chem. Preprints, 1982, ***27***, 244.

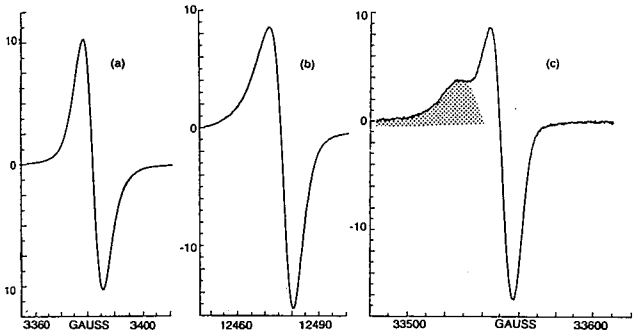

Figure 1. First evidence that VHF EPR can resolve sulfur-related spectral features in coal. (a) 9.5 GHz, (b) 35 GHz, (c) 96 GHz. Shaded area is the sulfur-related region.

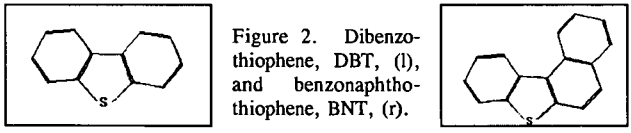

Figure 2. Dibenzothiophene, DBT, (l), and benzonaphthothiophene, BNT, (r).

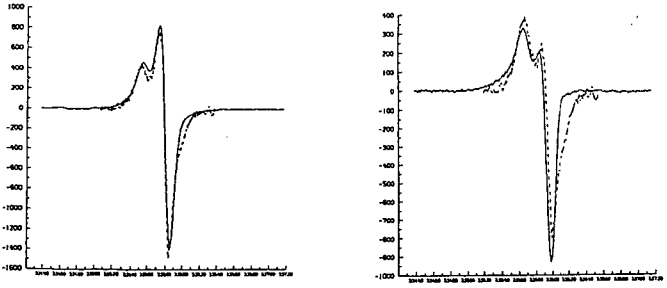

Figure 3. (a) Vitrinite, 2.9% organic S; (b) Sporinite, 4.3% organic S.

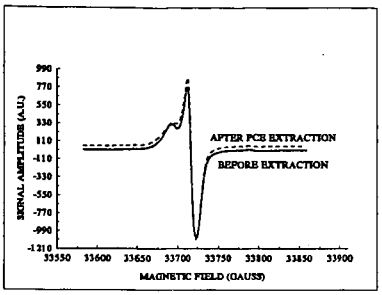

Figure 4(a). VHF EPR spectra of an Illinois #6 before (___) and after (---) PCE extraction.

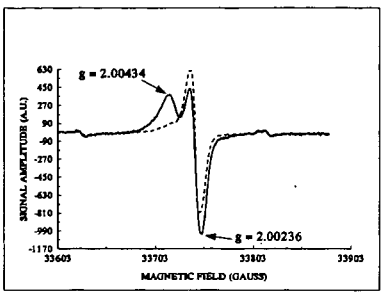

Figure 4(b). Illinois #6 coal before (___) and after (---) low temperature pyrolysis.

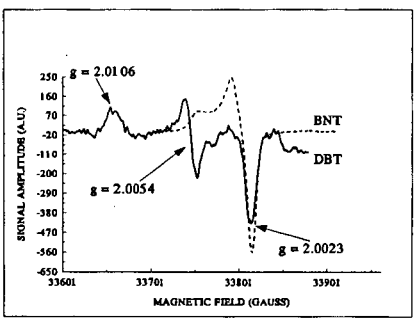

Figure 5. VHF EPR (ca. 96 GHz) spectra of DBT+ and BNT+ in boric acid glass.

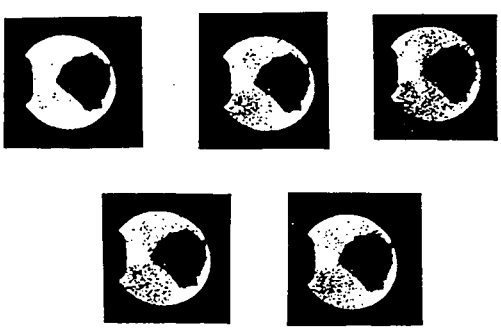

Figure 6. MRI images corresponding to five 1 mm. thick slices through an Illinois #5. Since water does not swell coal, this experiment defines the outer surface of the coal sample.

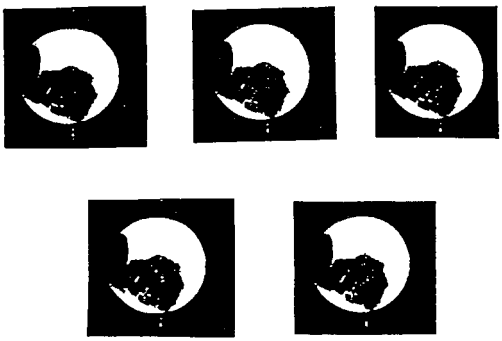

Figure 7. Same sample as in Fig. 6, but with acetone now as the solvent. A small degree of diffusion and swelling is observed.

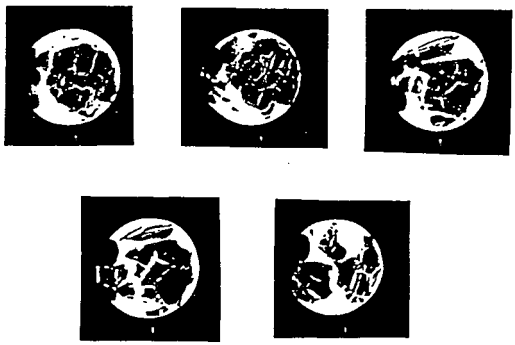

Figure 8. Same sample, now with DMSO as the solvent. Pore enlargement and swelling are now clearly visible.

NMR IMAGING: A 'CHEMICAL' MICROSCOPE FOR COAL ANALYSIS

D. C. French, S. L. Dieckmant, N. Gopalsamit, and R. E. Botto
Chemistry Division and †Materials and Components Technology Division
Argonne National Laboratory
9700 So. Cass Avenue
Argonne, IL 60439

Keywords: NMR, Imaging, Coal

ABSTRACT

This paper presents a new three-dimensional (3-D) nuclear magnetic resonance (NMR) imaging technique for spatially mapping proton distributions in whole coals and solvent-swollen coal samples. The technique is based on a 3-D back-projection protocol for data acquisition, and a reconstruction technique based on 3-D Radon transform inversion. In principle, the 3-D methodology provides higher spatial resolution of solid materials than is possible with conventional slice-selection protocols. The applicability of 3-D NMR imaging has been demonstrated by mapping the maceral phases in Utah Blind Canyon (APCS #6) coal and the distribution of mobile phases in Utah coal swollen with deuterated and protic pyridine.

INTRODUCTION

Coals are comprised of microscopically discernible regions (termed macerals) corresponding to different plant materials that have been geologically altered over time.[1] These discrete regions are known to exhibit widely different chemical behavior, thereby complicating coal processing technologies for the production of usable, high quality fuels and chemicals.

NMR imaging is sensitive to local chemical environments in complex molecular solids. Moreover, the technique has the unique capability of spatially mapping a sample's chemical or physical properties independently. Two-dimensional NMR imaging has proven to be a promising tool for the characterization of macerals in a dried specimen of Utah Blind Canyon coal.[2] However, a major difficulty in obtaining adequate spatial resolution in the third dimension rests with the intrinsic NMR properties, i.e., broad line widths, that are characteristic of many solids.

In this paper, we describe a 3-D NMR method that is based on a back-projection protocol in combination with image reconstruction techniques based on 3-D Radon transform inversion. Similar techniques have been described previously for imaging of liquid samples.[3,4] The method incorporates the experimental flexibility to overcome the difficulties which are presented by broad-line materials.

EXPERIMENTAL METHODS

The NMR imaging system used in this study consisted of a Bruker CXP-100 NMR spectrometer fitted with a home-built imaging accessory which is described in detail elsewhere.[5] The accessory, designed specifically for examining solid materials, consists of a versatile home-built IBM-PC based pulse programmer, three (X,Y,Z) Techron audio range 1-kW gradient amplifiers, a RF shaping unit, and a home-built, singly-tuned imaging probe capable of operating at 1-kW RF levels. The probe also contains forced-air-cooled gradient coils capable of operating with duty cycles in excess of 20% while producing a higher linear magnetic field gradient of 58 G/cm over a spherical space of 30 mm in diameter.

In a conventional 2-D NMR back-projection tomographic experiment, one applies a linear magnetic field gradient in a plane at numerous projection angles. For each angle, the Fourier transform of the data represents a planar integral of the proton density normal to the gradient vector. Similarly, in the 3-D back-projection experiment, by varying the gradient vector in order to sample the entire 3-D space, one obtains a 3-D Radon transform of the proton density. Let Rf(P) be the Radon transform of the object function f(M), where P and M are discrete points in the Radon and object space, respectively (Fig. 1).

$$Rf(P) = \int_{(OP.OM)=0} f(M)dM \qquad (1)$$

The inversion of this transform can be obtained by double differentiation and back projection. Marr et al.[6] have shown that the fastest way to invert the Radon transform is to use two sets of back projections, one along the meridian planes and the other along planes of constant latitude. The inversion can then be written as (Fig. 2):

$$f(M) = \frac{1}{4\pi}\int_{\theta=0}^{\theta=\pi}\int_{\phi=0}^{\phi=\pi}\frac{\partial^2 Rf}{\partial\rho^2}(\rho(M,\theta,\phi),\theta,\phi)sin\theta d\theta d\phi \qquad (2)$$

where ρ, θ, ϕ are the classical parameters of spherical coordinates, and $\rho(M,\theta,\phi) = OM \cdot n$, where O is the origin and n is the unit vector in the direction (θ,ϕ). The reconstruction algorithm of the 3-D Radon transform inversion was implemented as proposed by Grangeat and coworkers.[7]

Three-dimensional NMR imaging data were acquired on specimens using 128 complex data points, and a total of 3600 projections (30 θ angles over $\pi/2$ radians x 120 ϕ angles over 2π radians). A gradient strength of 25 G/cm and a sweep width of 200 kHz were used. A total of 64 averages were acquired by using an approximate 90° pulse and a recycle delay time of 0.25 s. A spectroscopic resolution of 80_x x 80_y x 80_z μm^3 was achieved. A total of 9 hours was required for data acquisition using these parameters.

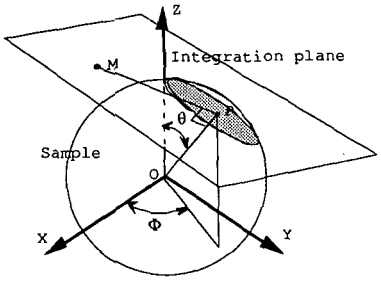

Fig. 1. Definition of 3-D Radon transform. Value of 3-D Radon transform in P is the integral of points M in plane defined by OP⊥MP.

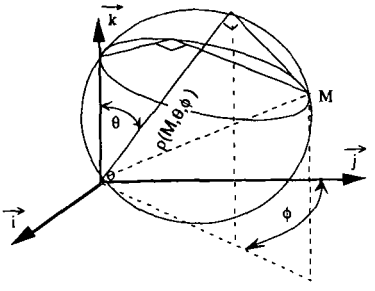

Fig. 2. Decomposition of integral over a sphere in two series of back-projections.

RESULTS AND DISCUSSION

In an earlier study, we had demonstrated the use of multi-pulse proton decoupling and back-projection reconstruction imaging methods to spatially resolve macroscopic resinite and vitrinite regions within a dried sample of Utah Blind Canyon coal.[2] Image contrast between the maceral phases was achieved on the basis of differences in proton density or spin-lattice relaxation (T_1). In the present study, we focus on the effects of solvent penetration to the swelling behavior of Utah coal.

The proton NMR spectrum of a specimen of Utah Blind Canyon coal swollen with "100%" deuterated pyridine is shown in Fig. 3. The spectrum displays three distinct proton resonances: there is a broad resonance (ca. 27 kHz) that corresponds to rigid protons in the sample, and there are two relatively narrow resonances (see expanded region at upper right) that correspond to aromatic and aliphatic protons in mobile environments. Line simulation subspectra were calculated from the experimental data by using a Pascal line simulation program on the Aspect 3000 computer as shown in Fig. 3. Analysis of the broad and narrow components indicates that approximately 14% of the protons are in the mobile phase. The fraction aromaticity (f_a^H) of protons in this mobile phase is calculated from line simulation as 0.45, compared with a value of 0.24 obtained from proton CRAMPS analysis of the dried coal. Because residual protons of the deuterated pyridine are expected to contribute less than 0.1% of the total proton signal, one can conclude that pyridine mobilizes highly aromatic regions within Utah coal preferentially.

A 3-D surface-rendered NMR image of the Utah coal specimen swollen with deuterated pyridine is shown in Fig. 4. The image was recorded with a short recycle-delay time in order to suppress signal from the broad "solid" component having a longer T_1. Thus, the image displays the proton distribution of mobile phases within the coal specimen preferentially. Surface rendering is performed by applying a user-adjusted threshold intensity to define a minimum intensity that is used to calculate the contiguous surface. The particular threshold employed was chosen to give the most accurate representation of the sample topology while suppressing low signal-to-noise structures near the sample surface. The image displayed is a good representation of the topology of the coal specimen; however,

it should be realized that surface features seen in the image represent areas with more or less density of mobile protons. For example, the feature seen at the front left of the object (indicated by arrow) is a crack in the specimen resulting from swelling with pyridine. Other features on the surface may be due to regions where there is a higher density of solid phase.

An 80-micron thin section (slice) of the 3-D NMR reconstructed image taken as a horizontal plane near the center of the specimen is shown in Fig. 5. Areas of bright intensity represent highly mobile regions within the specimen. Low intensity regions indicate solid phases or voids within the coal. The crack is clearly visible at the lower right portion of the image (indicated by arrow).

SUMMARY

We have demonstrated the feasibility of performing microtomographic NMR imaging on solid materials in three spatial dimensions. Methods were developed which combined 3-D back-projection protocol with image reconstruction using a Radon transform inversion technique. Using this methodology, we were able to spatially map maceral phases within a solid Utah coal specimen and monitor the distribution of mobile phases created upon swelling the specimen with pyridine.

ACKNOWLEDGMENTS

This work was performed under the auspices of the Office of Basic Energy Sciences, Division of Chemical Sciences, U.S. Department of Energy, under contract number W-31-109-ENG-38, and by the U.S. Department of Energy, Assistant Secretary for Conservation and Renewable Energy, Office of Transportation Systems, as part of the Ceramic Technology for Advanced Heat Engines Project of the Advanced Materials Development Program, contract number ACK-85234.

REFERENCES

1. *Chemistry and Characterization of Coal Macerals*; Winans, R.E. and Crelling, J.C., Eds.; ACS Symposium Series 252, American Chemical Society: Washington, D.C., 1984.
2. Dieckman, S.L.; Gopalsami, N; Botto, R.E. *Energy and Fuels* **1990**, *4*, 417.
3. Lauterbur, P.C.; Lai, C.-M. *IEEE Trans.* **1980**, *27*, 1227.
4. Lai, C.-M.; Lauterbur, P.C. *J. Phys. E.* **1980**, *13*, 747.
5. Gopalsami, N.; Foster, G.A.; Dieckman, S.L.; Ellingson, W.A.; Botto, R.E. *Development of NMR Imaging Probes for Advanced Ceramics*, Rev. Prog. in QNDE, Thompson, D.O. and Climenti, D.E., Eds.; Plenum Press, 1990.
6. Marr, R.B.; Chen. C.; Lauterbur, P.C. In *Aspects of Computerized Tomography*; Herman, G.T. and Natterer, F., Eds.; Springer-Verlag, 1980.
7. Grangeat, P.; Hatchadourian, G.; Le Masson, P.; Sire, P. *Logiciel Radon, Notice Descriptive Des Algorithmes Et Des Programmes*; Version 2.1 du 13-04-1990, LETI/DSYS/SETI/90-180 PS, Grenoble, 1990.

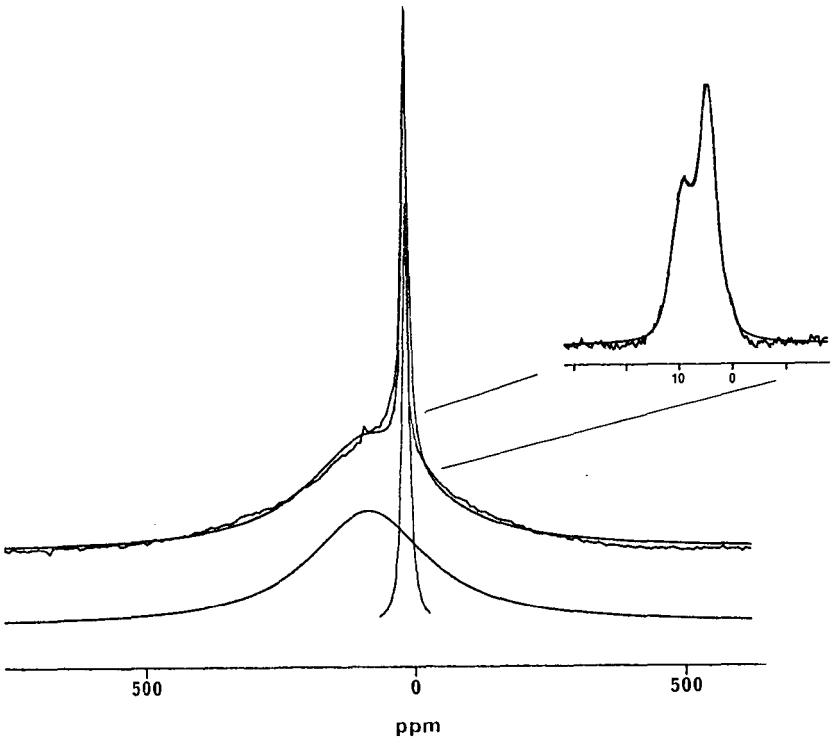

Fig. 3. Proton NMR spectrum of Utah Blind Canyon (APCS #6) coal specimen swollen with "100%" deuterated pyridine. Expanded plot at upper right displays narrow resonances with baseline correction applied.

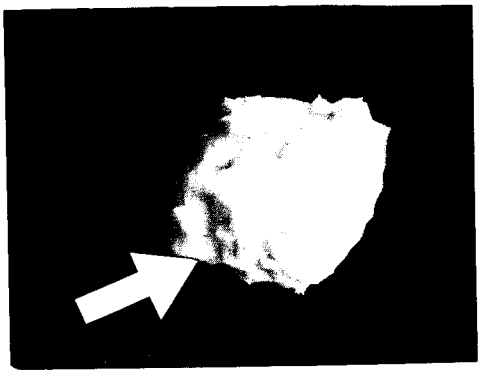

Fig. 4. Surface reconstructed 3-D NMR image of Utah Blind Canyon (APCS #6) coal specimen swollen with deuterated pyridine.

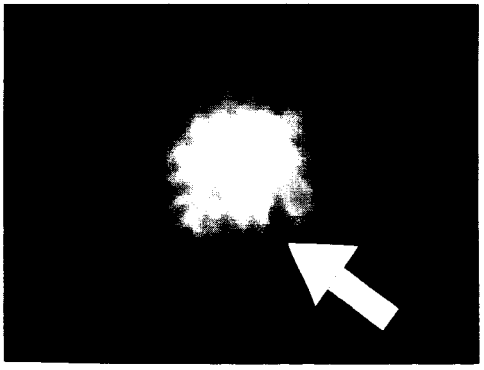

Fig. 5. Internal 2-D thin section of 3-D NMR reconstructed image of Utah coal specimen as shown in Fig. 4.

CHARACTERIZATION OF DELAYED COKING FEEDSTOCKS AND PRODUCTS BY ^{1}H AND ^{13}C NMR

Joaquin Rodriguez, John W. Tierney and Irving Wender
Chemical & Petroleum Engineering Department
University of Pittsburgh, Pittsburgh PA 15261

Keywords: Delayed coking, NMR spectroscopy, petroleum residues

ABSTRACT

^{1}H and ^{13}C nuclear magnetic resonance spectroscopy has been systematically applied to the characterization of delayed coking feedstocks (petroleum residues) as well as liquid products (naphtha, distillate, oils) and solid products (coke) to evaluate the type and extent of the cracking, polymerization and condensation reactions taking place. NMR results, combined with gas chromatography, elemental analysis and pilot plant data, yield mass balances at the atom-type level. A substantial increase in aromatic type carbons (40 wt%) occurs (for a particular feedstock), primarily at the expense of naphthenic type carbons (35 wt%), and is accompanied by a significant reduction in the number of protons attached to aromatic carbons (80 wt%). This methodology can be used to measure the severity of delayed coking and to estimate product yields and compositions.

INTRODUCTION

Delayed coking is the most widely used process for the conversion of petroleum residues[1]. Residues are pumped through a coker heater, where the temperature is raised to 450-500 ° C in a short period of time, and then fed into one of two coke drums (adiabatic reactors). Cracking, polymerization and condensation reactions, initiated in the heater, proceed forming vapors (gases, naphtha, oils) that leave the reactor and are sent to a fractionation tower. A highly viscous carbonaceous material remains in the drum and finally is transformed into a solid product (coke) which can be used (depending upon specifications) as fuel or as filler for the production of carbon anodes (aluminum industry) or arc-electric furnace electrodes (steel industry)[1,2].

Delayed coking feedstocks (vacuum and conversion petroleum residues) contain mainly aromatic hydrocarbons with aliphatic substituents, paraffins, naphthenic compounds and heteroatoms (mostly in heterocyclic compounds). The aromatic components are the network members of the final coke structure: higher aromatic contents give more extended aromatic arrangements and consequently better coke quality due to more ordered domains of oriented molecules[3]. On the other hand, reactivity of these feedstocks is related to the number of substituents attached to the aromatic compounds: high aromaticity with only a few substitutents (coal tar pitches) corresponds to low reactivity and moderate aromaticity with many substituents (vacuum residues) to high reactivity. A balance is desired for optimum carbonization[4].

Nuclear magnetic resonance (^{1}H and ^{13}C NMR) is a powerful technique to evaluate delayed coking feedstocks and the corresponding carbonization process, due to its ability to elucidate basic constituents present in these materials. ^{13}C NMR provides direct measurement of the types of carbon atoms which determine the pyrolysis chemistry[5]. Quantitative information is obtained by integrating line intensities. These are proportional to the number of carbon atoms of each type[6]. With additional information from ^{1}H

NMR, average molecular parameters can be derived, and even structural configurations can be drawn (only useful as illustrative tools because these materials embrace a large range of organic molecules as indicated by the broad molecular weight spectra). This constitutes a sound basis for understanding carbonization mechanisms and for comparing different delayed coking feedstocks.

EXPERIMENTAL

Delayed coking products were obtained in a thermal conversion pilot plant with a 4 lt. reactor capacity operating in continuous up-flow mode at 1500-2000 g/h, 60-140 psig and internal temperature profiles between 400-500 ° C. Gas product was monitored by gas chromatography every 20 minutes and the weighted average reported. Liquid product collected during operation was characterized and later distilled in consecutive ASTM D-86 and D-1160 assays to yield four fractions: naphtha (IBP-400 F), distillate (400-650 F), light oil (650-800 F) and heavy oil (800 F+). Coke was recovered after cooling the reactor.

NMR spectra were collected in a Bruker 300 MSL spectrometer. Liquid ^{13}C NMR spectra were obtained at 75.468 MHz in a 10 mm probe, using a gated program with decoupler on during acquisition and off during the rest of the experiment to suppress the Nuclear Overhauser Effect. Relaxation times of 5 to 10 seconds were used, 45 pulse angle (corresponding to 5 μs pulse time) and 31 μs for dead time delay. Resolutions of about 1.3 Hz were achieved with receiver gains of 10-30. Liquid ^{1}H NMR spectra were obtained at 300 MHz in a 5 mm probe with repeated pulses of 6.1 μs. Band assignments for integrating atomic groups were selected from the extended consensus in the field (reference to TMS standard)[5,7-8]:

	^{13}C NMR		^{1}H NMR	
Aromatics	110-160 ppm	Aromatics	6.5 -9.0	ppm
-protonated	110-130 ppm	-single ring	6.5 -7.25	ppm
-quaternary	130-160 ppm	-multi. ring	7.25-9.0	ppm
Aliphatics	5- 60 ppm	Aliphatics	0.5 -4.0	ppm
-paraffinics	5- 25 ppm +	-terminal CH_3	0.5 -1.0	ppm
	25- 60 ppm peaks	-internal	1.0 -1.8	ppm
-naphthenic	25- 60 ppm envelope	-α aromatic C	1.8 -3.8	ppm
Olefinic	80-100 ppm	Olefinic	4.5 -6.3	ppm

Gas chromatography data were converted to a similar atom type distribution. Solid state MAS $^{13}C/^{1}H$ cross-polarization spectra (for cokes)[9-10] were obtained at 75.473 MHz and 3500-4000 rpm spinning rates with a proton enhanced pulse program (PENMR).

RESULTS AND DISCUSION

Pilot plant data include the distribution of product yields and basic characteristics of feedstocks and products (Table 1). ^{1}H and ^{13}C NMR spectra for feedstocks and liquid products are presented in Figures 1-6.

A solid state NMR spectrum for coke is presented in Figure 7. It shows an aromatic carbons peak at the center (100-150 ppm) and two pairs of side-bands. This indicates that only quaternary aromatic carbons and protonated aromatic carbons (that have been calculated to match C/H ratios) are present.

NMR data have been integrated into a weighted distribution (Table 2) and is

compared with the feedstock analysis (Table 3) to determine the differences and to calculate changes (defined by Difference*100/Feedstock).

It is observed that a significant increase in aromatic carbons (39.4 wt%) occurs, mainly at the expense of a reduction in the naphthenic carbons (-35.0 wt%) with small changes in protonated aromatic carbons (8.5 wt%) and paraffinic carbons (-3.8 wt%). This can be interpreted to mean that the main polymerization/condensation mechanism involves aromatization of naphthenic rings attached to aromatic rings (in this case probably in a 1/1 ratio).

Also, the substantial reduction in protons attached to aromatic carbons (mainly in multiple ring systems) suggests that the carbonization reactions in the liquid phase (leading to coke formation) proceed through benzyl type radicals, while in the vapor phase, cracking reactions substantially reduce the size of the molecules, bringing complex high boiling compounds (present in the feedstock) down to lighter molecules (gas, naphtha, oils).

CONCLUSIONS

A systematic application of ^{13}C and ^{1}H NMR analysis to delayed coking feedstocks and products results in a quantitative evaluation of the polymerization/condensation reactions and can be used as a measurement of the severity of the process and to estimate product composition.

BIBLIOGRAPHY

1. **Feintuch, H.M. et al.**, in Handbook of petroleum refining, R.A. Meyer (ed), pp. 3-61 (1986).
2. **De Biase, R. et al.**, in Petroelum Derived Carbons, ACS, pp. 155-171 (1986).
3. **Winter, L.L.**, Kirk-Othmer Enc. Chem. Tech., pp.570-576 (1978).
4. **Mochida, I. et al.**, Oil Gas J. 86(18):73-77 (1988).
5. **Seshadri, K.S. et al**, Fuel, 61(4):336-340 (1982).
6. **Gillet, S. et al.**, Fuel, 60(3):221-225 (1981).
7. **Cookson, D.J. and Smith, B.E.**, in Coal Science and Chemistry, A. Volborth (ed), pp. 31-60 (1987).
8. **Yamashita, G.T. et al.**, Preprints ACS Div. Petroleum Chem., 34, (2) 301-305 (1989).
9. **Nakamizo, M. and Adacchi, Y.**, 19th Bienn. Conf. Carbon, pp. 148-149 (1989).
10. **Hinckley, C.C. et al.**, SIU Carbondale, Sixth Ann. Conf. Mater. Techn. Center, pp. 14-31 (1990).

ACKNOWLEDGEMENTS

This work has been financially supported by INTEVEP S.A. (R&D Center of Petroleos de Venezuela). Special thanks are due to Mr. Carlos Mota, project leader. Also we appreciate the assistance of Dr. Lurie Galya and Dr. George Marcelin in the operation of the NMR instrument.

Table 1. Delayed coking pilot plant data

Material	Yield wt%	Boiling range, ° F	API gravity	Impurities wt%
Feedstock	-	350-600	14.6	3.03
Gases	10.31	-	-	0.22
Naphtha	24.66	IBP-400	57.9	0.25
Distillate	26.57	400-650	30.2	1.88
Light Oil	12.33	650-800	15.3	3.24
Heavy Oil	7.84	800+	4.6	3.88
Coke	18.28	-	-	4.47

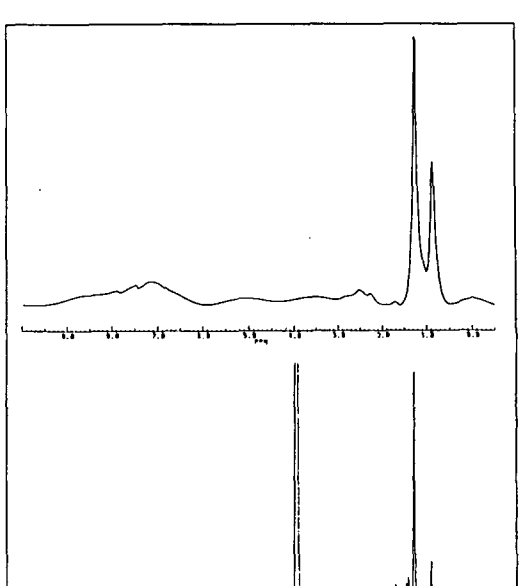

Figure 1. ^{1}H and ^{13}C NMR spectra of a delayed coking feedstock

Table 2. Distribution of proton and carbon atoms in delayed coking products

Atom type wt%	Gas wt%	Naphtha wt%	Distillate wt%	Light Oil wt%	Heavy Oil wt%	Coke
CARBON	8.12	21.54	23.01	10.67	6.80	17.28
Aromatic	0.00	4.27	6.14	4.18	3.26	17.28
-protonated	0.00	2.13	2.95	2.10	1.73	2.16
-quaternary	0.00	2.14	3.20	2.07	1.53	15.12
Aliphatic	7.64	17.28	16.87	6.50	3.55	0.00
-paraffinic	7.64	13.83	10.14	4.03	2.36	0.00
-naphthenic	0.00	3.45	6.72	2.47	1.19	0.00
Olefinic	0.48	0.00	0.00	0.00	0.00	0.00
PROTON	1.98	3.06	3.06	1.26	0.74	0.18
Aromatic	0.00	0.12	0.17	0.19	0.13	0.18
-single	0.00	0.07	0.11	0.06	0.03	0.00
-multiple	0.00	0.05	0.07	0.13	0.10	0.18
Aliphatic	1.88	2.83	2.83	1.04	0.59	0.00
-terminal	1.58	1.15	0.84	0.24	0.12	0.00
-internal	0.31	1.47	1.57	0.58	0.34	0.00
-α arom. C	0.00	0.20	0.41	0.22	0.13	0.00
Olefinic	0.06	0.11	0.06	0.03	0.01	0.00

Table 3. Atom type balances in delayed coking reactions

Atom type	Feed wt%	Products wt%	Difference wt%	Change %
CARBON	85.99	87.43	+ 1.44	+ 1.68
Aromatic	25.19	35.13	+ 9.93	+39.42
-protonated	10.20	11.07	+ 0.87	+ 8.53
-quaternary	15.00	24.06	+ 9.06	+60.40
Aliphatic	60.79	51.82	- 8.97	-14.76
-paraffinic	39.50	37.99	- 1.51	- 3.82
-naphthenic	21.29	13.83	- 7.46	-35.04
Olefinic	0.00	0.48	+ 0.48	+
PROTON	10.98	10.26	- 0.72	- 6.56
Aromatic	3.89	0.80	- 3.09	-79.52
-single	1.11	0.27	- 0.84	-75.85
-multiple	2.78	0.53	- 2.25	-80.98
Aliphatic	7.09	9.17	+ 2.07	+29.21
-terminal	2.14	3.93	+ 1.79	+83.52
-internal	4.37	4.27	- 0.10	- 2.22
-α arom. C	0.58	0.96	+ 0.38	+65.37
Olefinic	0.00	0.27	+ 0.27	+
H2	-	0.03	+ 0.03	+

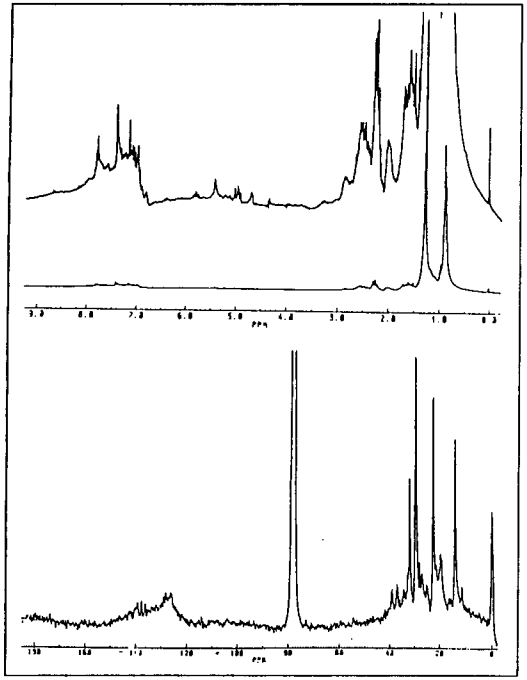

Figure 2. ^{1}H and ^{13}C NMR spectra of a delayed coking liquid product

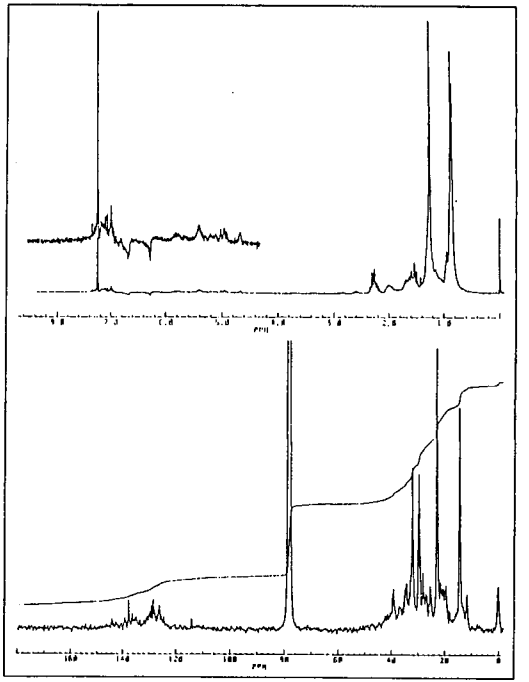

Figure 3. ^{1}H and ^{13}C NMR spectra of a delayed coking naphtha

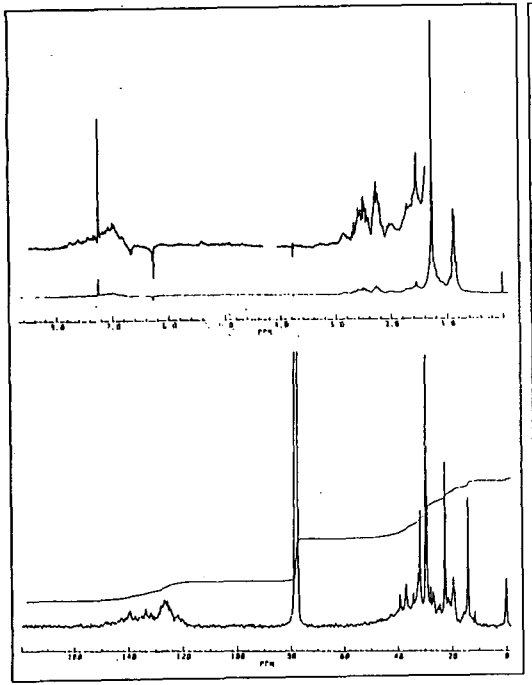

Figure 4. ^{1}H and ^{13}C NMR spectra of a delayed coking distillate

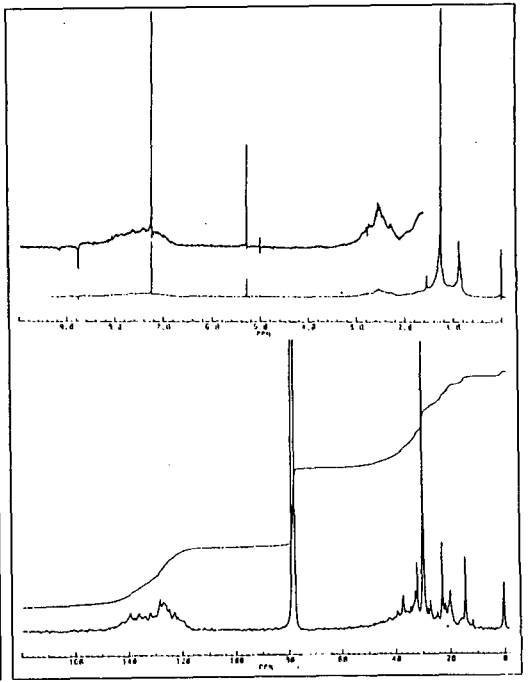

Figure 5. ^{1}H and ^{13}C NMR spectra of a delayed coking light oil

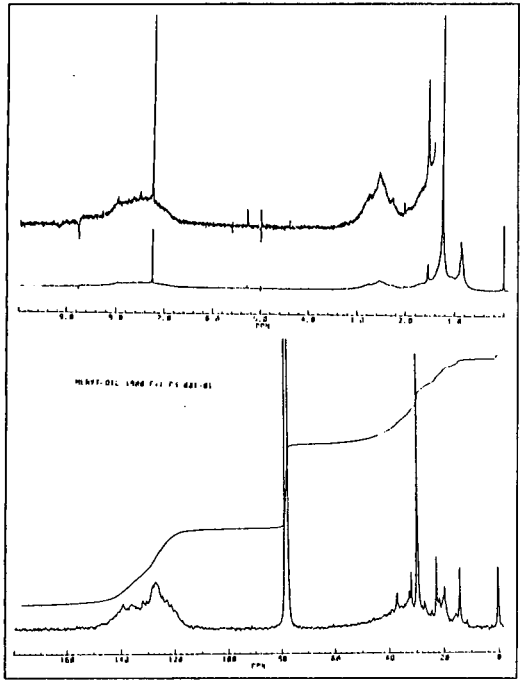

Figure 6. ^{1}H and ^{13}C NMR spectra of a delayed coking heavy oil

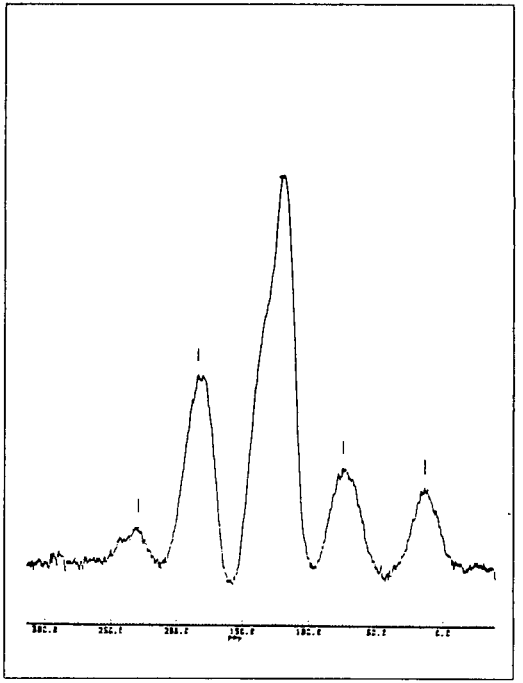

Figure 7. $^{13}C/^{1}H$ crosspolarized MAS solid NMR spectrum of a petroleum coke

THE DETERMINATION OF LOCAL STRUCTURE IN ORGANOFLUORIDES USING FLUORINE-19 CARBON-13 DIPOLAR COUPLING

Edward W. Hagaman
Chemistry Division, Oak Ridge National Laboratory
Oak Ridge, Tennessee 37831

Keywords: Solid State NMR, ^{19}F-^{13}C Dipolar Coupling, Fluorinated Coal

INTRODUCTION

A facet of our research has been directed toward the elucidation of "reactive sites" in the organic milieu of coals. The conceptual framework for these experiments is the chemical introduction of a unique, NMR active nucleus at or adjacent to a reactive site in the coal network and the subsequent utilization of this nucleus to extract site specific structural information by solid state ^{13}C NMR spectroscopy. Fluorine-19 and phosphorus-31 nuclei are good NMR choices, having large magnetic moments, 100 % natural abundance, and spin 1/2. The absence of a quadrupole moment translates into narrow, well-resolved spectral resonances. Both are suitable in applications to coal derivatization, having small natural concentrations in the organic matrix of most coals.[1] Fluorine is attractive from the standpoint of chemical manipulation of coals in that a large and increasing number of fluorinating reagents are available to specifically incorporate fluorine into organic substances. It should be possible to label diverse sites in the coal by a judicious choice of fluorinating reagent and reaction conditions.

The use of an introduced magnetic nucleus in an organic environment as a probe of local structure utilizes in some fashion the dipolar interaction between the probe nucleus and proximate ^{13}C nuclei to selectively observe the interactive carbons. Since ^{13}C is dilute by virtue of low natural abundance, these dipolar couplings are often isolated spin pair interactions. Two experiments that selectively detect carbons dipolar coupled to a probe nucleus are cross polarization between the nuclear pair, and dephasing of ^{13}C magnetization by interference with rotational echo formation. The first class of experiments are known as double cross polarization (DCP) NMR[2,3]; the second as rotational-echo double resonance (REDOR) NMR[4]. This paper reports experiments that demonstrate the REDOR experiment is ineffective when applied to the ^{19}F-^{13}C nuclear pair in models of molecular weight < 300. A new experiment that uses the cause for the REDOR failure, ^{19}F spin diffusion, is used to regain site specific structural information encoded by the ^{19}F-^{13}C dipolar coupling.

RESULTS AND DISCUSSION

We have examined the perturbation of the conventional CP/MAS ^{13}C NMR spectrum of organic substances due to the incorporation of a of a single ^{19}F atom in the structure. In molecules in which the

fluorine atom undergoes little motion in the solid, e.g., as in 16α-fluoroestrone-3-methyl ether, (1), the carbon directly bonded to fluorine has a resonance so broad (> 2500 Hz) that it is not observed in the spectrum. In molecules that exhibit motion in the crystal that modulates the ^{19}F-^{13}C dipolar interaction, as in ortho-fluorophenylglycine, the ^{19}F-^{13}C dipolar coupling is partially averaged by the motion and the directly fluorinated carbon is observed. In this case the resonance is narrowed enough that the J-coupling (250 Hz) between the directly bonded pair is apparent in the conventional spectrum. Longer range ^{19}F-^{13}C dipolar interactions result in a graded, r^{-3} internuclear distance dependent broadening of near neighbor carbon resonances in the spectrum. Simultaneous ^{1}H and ^{19}F high power decoupling applied during the free induction decay acquisition time efficiently eliminates heteronuclear dipolar coupling from the spectrum. This triple resonance capability is required to obtain high quality CP/MAS ^{13}C NMR spectra on organofluorides obtained at routine (< 5 kHz) MAS speeds.

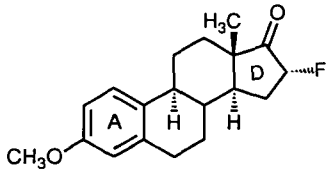

1

The spectral response described above may not be anticipated on first glance since the dipolar interaction between two spin 1/2 nuclei has the form $(r^{-3})(3\cos^2\theta-1)$ and should be averaged to zero by MAS. However, MAS is successful only when the rotation rate is large in comparison to the dipolar interaction linewidth. The maximum dipolar linewidth, $2D_{CF}$, for a directly bonded pair is about 26 kHz, the consequence of the large magnetic moment of F19 and short C-F bond distance ($r \approx 0.13$ nm). In this instance the actual 4.2 kHz spinning used in these experiments is ineffective. This MAS speed is just comparable to typical ^{19}F-^{13}C dipolar linewidths for atoms separated by two bonds ($r \approx 0.23$ nm, $D_{CF} \approx 4.5$ kHz). In the absence of ^{19}F dipolar decoupling, these resonances have a ca. 50 Hz residual linewidth contribution due to incomplete averaging of the dipolar interaction by MAS.

The REDOR experiment requires that the dipolar coupled spin pair (^{19}F-^{13}C in the present case) in a system be isolated. If so, the time average of the resonance frequencies over one MAS rotor period is zero, i.e., full recovery of signal intensity occurs after each rotor cycle, producing a train of rotational echoes. REDOR uses π pulses applied to the probe nucleus (^{19}F) to intentionally cause echo destruction of those ^{13}C resonances dipolar coupled to ^{19}F. These are detected in a difference experiment. In 1, for example,

the anticipated REDOR difference spectrum would contain only ring D carbon resonances with intensities that reflect an r^{-3} distance dependence. The placement of π pulses and signal acquisition are timed to rotor position; REDOR signals can be accrued over even, integral multiples of the rotor cycle.[5]

Attempts to perform REDOR on **1** and smaller molecules has met with marginal success in our laboratory. Initial REDOR difference signal intensities in 3-fluoro-4-methoxybenzoic acid (evolution for two rotor cycles) do not exhibit the expected intensity ratios based on ^{19}F-^{13}C internuclear distance. The resonances of C(2) and C(4) have greater integrated areas than the fluorinated carbon resonance, C(3). Continued evolution (4-20 rotor cycles) yields a strong selective attenuation of the REDOR signal set. We have shown in separate ^{13}C T_2 experiments, with and without ^{19}F decoupling, that the signal decay is governed by the ^{19}F T_2. In effect, ^{19}F intermolecular spin diffusion provides a dephasing mechanism for coupled ^{13}C nuclei that competes with the experimentally imposed π pulses of REDOR, violating the isolated pair precondition in this experiment. This failure mode has been observed in ^{15}N-^{13}C REDOR experiments in which spin diffusion among ^{13}C nuclei defeat the REDOR difference signal.[6]

For isolated spin pairs, REDOR accesses the dipolar interaction between the pairs, and, hence, is a direct method to obtain structural information. This experiment will work for the ^{19}F-^{13}C pair in high molecular weight molecules where ^{19}F spin diffusion is suppressed by large internuclear distances. The applicability of this experiment in coal structure analysis is great for chemical derivatizations that introduce low concentrations of fluorine into the material. For more highly fluorinated coals, an new experiment has been created that uses the dipolar interaction to provide site selective structural information. The experiment accrues the difference signal between spectra that measure C13 T_2 over even integral multiples of the rotor period (to allow refocussing of ^{13}C chemical shift anisotropy), with alternate scans employing ^{19}F heteronuclear decoupling during the rotor evolution period. Signals arise from those carbons that show differences in T_2 arising from ^{19}F-^{13}C dipolar dephasing mediated by the ^{19}F spin diffusion. Carbon signal intensities in this T_2 difference map do not provide a direct measure of ^{19}F-^{13}C dipolar coupling. The structural information that can be gleaned from this and related experiments is under current investigation. Further studies are planned to delineate ^{19}F internuclear distance boundaries that are appropriate for these experiments.

ACKNOWLEDGEMENTS

This research was sponsored by the Division of Chemical Sciences, Office of Basic Energy Sciences, U. S. Department of Energy under contract DE-AC05-840R21400 with Martin Marietta Energy Systems, Inc.

REFERENCES
1. Hagaman, E. W. Energy & Fuels **1988**, 2, 861-862.

2. For C13-N15 cross polarization: (a) Schaefer, J.; McKay, R. A.; Stejskal, E. O. J. Magn. Reson. **1979**, 34, 443-447.
(b) Stejskal, E. O.; Schaefer, J.; KcKay, R. A. J. Magn. Reson. **1984**, 57, 471-485. (c) Schaefer, J.; Stejskal, E. O.; Garbow, J. R.; McKay, R. A. J. Magn. Reson. **1984**, 59, 150-156.

3. For C13-P31 cross polarization: (a) Hagaman, E. W.; Ho, P. C.; Brown, L. L.; Schell, F. M.; Woody, M. C. J. Am. Chem Soc. **1990**, 112, 7445-7450. (b) Hagaman, E. W. Energy & Fuels **1988**, 2, 861-862.

4. Gullion, T.; Schaefer, J. J. Magn. Reson. **1989**, 81, 196-200. Marshall, G. R.; Beusen, D. D.; Kociolek, K.; Redlinski, A. S.; Leplawy, M. T.; Pan, Y.; Schaefer, J. J. Am. Chem.Soc. **1990**, 112, 963-966.

5. Gullion, T.; Poliks, M. D.; Schaefer, J. J. Magn. Reson. **1988**, 80, 553-558.

6. Christensen, A. M.; Schaefer, J., private communication.